Chem Catalysis

Article

Benchmarking photocatalysts for dinitrogen photoreduction reaction

Graphical abstract

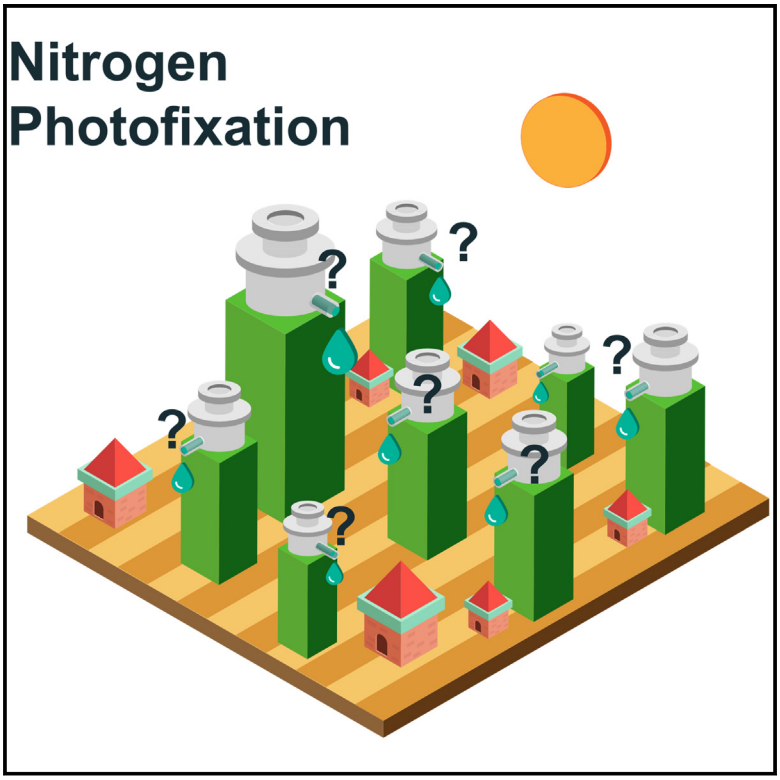

Highlights

- Identify key nitrogen contamination sources for photocatalytic nitrogen fixation
- Suggest essential controls for standardizing NH_3 measurements in the pNRR field
- Reiterate the importance of strict testing procedures and promote reproducibility testing

Authors

Po-Wei Huang, Danae A. Chipoco Haro, Hakhyeon Song, Andrew J. Medford, Marta C. Hatzell

Correspondence

ajm@gatech.edu (A.J.M.), marta.hatzell@me.gatech.edu (M.C.H.)

In brief

This work revisits photocatalysts from the literature that have previously been reported as active for the photocatalytic nitrogen reduction reaction (pNRR). We identified key nitrogen contamination sources in pNRR and customized a photochemical setup with ultra-low nitrogen impurities to conduct rigorous pNRR experiments. In our system, these photocatalysts exhibit negligible activity for photocatalytic ammonia production. Essential control experiments were suggested to help the field elucidate the genuine photoactivity toward pNRR.

Huang et al., 2024, Chem Catalysis *4*, 101128
October 17, 2024
https://doi.org/10.1016/j.checat.2024.101128

CellPress

Chem Catalysis

CellPress

Article

Benchmarking photocatalysts for dinitrogen photoreduction reaction

Po-Wei Huang,[1] Danae A. Chipoco Haro,[2] Hakhyeon Song,[3] Andrew J. Medford,[1,*] and Marta C. Hatzell[1,3,4,*]
[1]School of Chemical and Biomolecular Engineering, Georgia Institute of Technology, Atlanta, GA 30332, USA
[2]School of Materials Science and Engineering, Georgia Institute of Technology, Atlanta, GA 30332, USA
[3]George W. Woodruff School of Mechanical Engineering, Georgia Institute of Technology, Atlanta, GA 30332, USA
[4]Lead contact
*Correspondence: ajm@gatech.edu (A.J.M.), marta.hatzell@me.gatech.edu (M.C.H.)
https://doi.org/10.1016/j.checat.2024.101128

THE BIGGER PICTURE Ammonia (NH_3) is important for producing synthetic fertilizers to sustain the growing global population. The current process for NH_3 production (Haber-Bosch process) produces 500 million tons of CO_2 each year. Photocatalytic nitrogen reduction reaction (pNRR) for ammonia production does not involve a carbon source and relies on available feedstocks: energy from sunlight, water as a proton source, and air as a nitrogen source. The pNRR is widely reported, but one of the main challenges in pNRR research is to detect NH_3 reliably due to adventitious NH_3 contamination and nitrogen-containing impurities. We developed a setup to suppress adventitious nitrogenous contaminants and benchmark three photocatalysts. Our results suggest that standardization of NH_3 measurements in the pNRR field is critical to ensuring reliable results.

SUMMARY

The photocatalytic nitrogen reduction reaction (pNRR) for ammonia (NH_3) production is often discussed as a sustainable alternative to the thermocatalytic Haber-Bosch process. One of the main challenges in pNRR research is the lack of reliable detection of photochemically produced NH_3 since NH_3 concentrations are often low and nitrogen-containing impurities may be present. Here, we identify three key sources of contamination (feed gases, catalyst precursors, and hole scavengers) and systematically quantify and reduce the contamination. We developed a custom photoreactor setup to minimize contamination and benchmarked three photocatalysts previously reported to be active toward pNRR. Our results indicate that the pNRR rates of all three catalysts under benchmarking conditions are much lower than previously reported and in some cases have negligible activity. We suggest essential control experiments to contribute to the standardization of NH_3 measurements in the pNRR field and to help the field elucidate the photoactivity of catalysts toward pNRR.

INTRODUCTION

Nitrogen-based fertilizers (e.g., potassium nitrate, ammonia, urea) have had a profound impact on modern society by ensuring food production. Throughout history, these fertilizers have relied heavily on natural sources such as bird guano or coke deposits.[1,2] In the 20th century, concerns about the ability of naturally sourced fertilizers to sustain the continuously growing population prompted research on the development of synthetic fertilizers.[3] One early idea, pioneered by Dhar's group in 1941, was the suggestion of light-assisted NH_3 production in soils.[4] In 1977, this idea was advanced when Schrauzer and Guth reported the conversion of N_2 into NH_3 through a photocatalytic reduction over TiO_2.[5] This breakthrough sparked great research interest in the photocatalytic nitrogen reduction reaction (pNRR).[6–8] However, subsequent studies led to divergent findings. In 1992, Edwards et al. first raised the concern about the effect of adventitious NH_3 contamination on the interpretation of experimental results.[9] This cast doubt on the feasibility of pNRR and sparked a contentious debate in *Angewandte Chemie*.[10–12] The lack of consensus and the successful industrialization of NH_3 synthesis via the Haber-Bosch process led to a decline in studies of pNRR in the decades following.

Current NH_3 production occurs through the Haber-Bosch process, a thermocatalytic process that converts N_2 and H_2 into NH_3. This process is associated with 500 million tons of annual CO_2 emissions, mainly due to its reliance on fossil hydrocarbons (coal or methane) to produce hydrogen feedstock.[13,14] To meet the Paris Agreement goal of net-zero CO_2 emissions by 2050, research is actively exploring carbon-neutral or carbon-negative alternatives for next-generation NH_3 production.[15,16] One approach that has already been deployed is to couple carbon

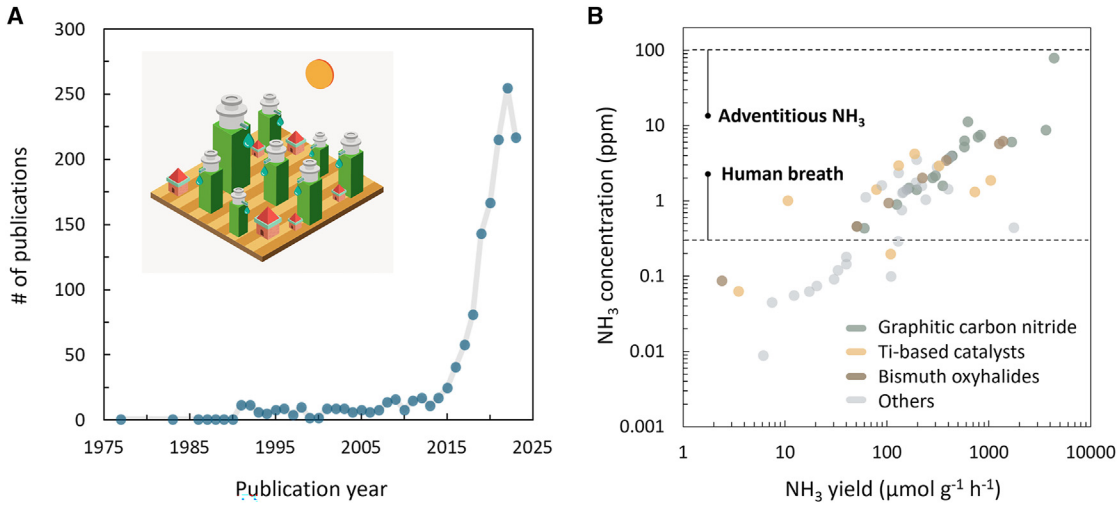

Figure 1. Current progress of nitrogen photofixation

(A) The number of published research articles on photocatalytic nitrogen reduction reaction from 1977 to 2023. The results were based on data from Web of Science, using the keywords nitrogen photofixation, nitrogen photoreduction, and photocatalytic nitrogen fixation. Inset of the figure is a schematic of distributed photocatalytic ammonia production.

(B) Reported photocatalyst activity toward ammonia production. The ammonia concentration is estimated after 1 h of photolysis. Data of human breath are from Andersen et al.[26] and data of adventitious ammonia is from Iriawan et al.[27]

capture/storage/utilization techniques with the Haber-Bosch plants to lower CO_2 emissions. Another approach is to replace the H_2 production in the Haber-Bosch process with renewable processes (e.g., water electrolysis or even photolysis). This pathway has gained much attention since it retains the high thermochemical efficiency of the Haber-Bosch process ($\geq$70% in industrial processes) while significantly reducing CO_2 emissions (theoretically, it can reach carbon-free NH_3 manufacturing).[17,18] The feasibility of renewable H_2 generation depends on the cost of electricity, the development of electrocatalytic water splitting, and the implementation of carbon tax. In the near future, we can expect the Haber-Bosch process paired with renewable H_2 to come on the market.[19] pNRR as another carbon-free pathway for the synthesis of NH_3 has regained attention (Figure 1A). Unlike the aforementioned sequential processes (where H_2 production and N_2 reduction reaction are separate processes), pNRR utilizes solar energy to directly convert water (the proton source) and air (the nitrogen source) into NH_3 and produces only environmentally friendly by-products (oxygen). Research has found the development of pNRR very attractive in the pursuit of process intensification and decentralized NH_3 production.[20–22] Additionally, the development of pNRR technology has also raised interest from the perspective of fundamental science development, since nitrogen photofixation is the process found in nature to regulate the global nitrogen cycle.[23–25]

The resurgence of pNRR research has also benefited from advances in modern photochemistry and catalyst design. Defects such as oxygen vacancies (OVs) are closely linked to the photocatalytic yield of NH_3, leading to the common hypothesis that OV is the active site for pNRR.[28,29] Additionally, materials with smaller band gaps (e.g., bismuth oxyhalides, graphitic carbon nitride) that respond to visible light have been reported to exhibit photoactivity toward pNRR.[30,31] Despite the development of photocatalysts for pNRR, the current NH_3 yield from photocatalytic routes remains low. The low yield makes the results susceptible to the influence of adventitious NH_3 contamination in the environment (Figure 1B). Concerns about false positives from adventitious NH_3 are not unfounded. Recent studies in electrocatalytic nitrogen reduction reaction (eNRR) have revealed that several catalysts, initially reported to be highly active, were later discovered to be inactive in reducing N_2.[26,32,33] Triggered by these irreproducible results, a series of discussions ensued, encompassing the identification and elimination of contamination sources, the development of reliable techniques for measuring low concentrations of ammonia, and the establishment of standardized testing protocols for the field.[26,27,34,35] Considering that current photocatalytic NH_3 yields are at least an order of magnitude lower than those achieved through electrocatalytic approaches, and given the additional concern regarding the photostability of nitrogen-containing photocatalysts,[36] the issue of contamination becomes even more critical in the field of pNRR.

Discussions on contamination have gradually gained attention in the field of pNRR, with proposed methodologies and good experimental practices to suppress adventitious NH_3.[27,35,37,38] Here, we take a step further to benchmark and reexamine some of the reported photocatalysts, leveraging the current knowledge of contamination issues and NH_3 quantification. We developed a setup aimed at suppressing contamination from feed gases, equipment/reactors, and catalysts. We synthesized three photocatalysts previously reported to have high activity for photocatalytic NH_3 synthesis (Fe-BiOBr, g-C_3N_4/Fe_2O_3, and OV-TiO_2) and tested their photoactivity using the custom setup with strict controls. The results indicate that NH_3 synthesized from N_2 is negligible in all cases. We suggest essential control experiments that should be used to ensure rigor and reproducibility within the field.

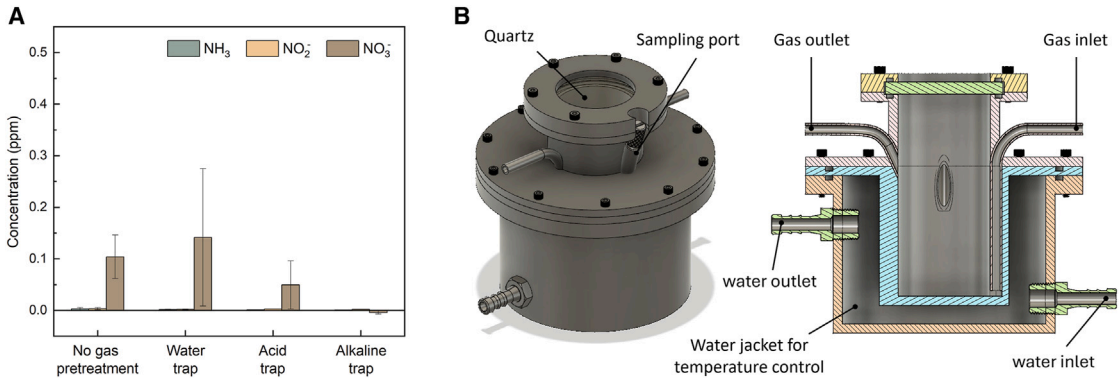

Figure 2. Decontamination efforts for pNRR

(A) Decontamination effects of various gas pretreatment methods. The error bars represent the SDs from three independent measurements.

(B) The design of a custom-built photoreactor and its cross-sectional diagram.

RESULTS AND DISCUSSION

Currently, there are no standardized testing protocols for pNRR.[38] We have chosen experimental parameters that are commonly used in the field or fall within the range described in the literature (e.g., 300-W Xenon lamp, solid-liquid suspension reactor, and 50 standard cubic centimeters per minute [SCCM] flow rate) for the evaluation of the photocatalyst (Table S1). Given the previously discussed concerns about contamination leading to false positive results, a crucial first step is to carefully inspect and remove any potential contaminants before evaluating the activity of the photocatalysts. Here, we discuss several key aspects of decontamination, such as feed gas treatment, reactor design, and cleaning procedures. Our objective is to minimize contamination interference and establish a rigorous photochemical system for pNRR benchmarking.

In pNRR studies, the feed gas (i.e., N_2) is the most common source of contamination. According to a previous report,[34] even with ultrahigh purity N_2 gas (99.999%), in the worst-case scenario where all impurities are assumed to be nitrogenous contaminants (NH_3 and NO_x) that can dissolve in the solvent, hundreds to thousands of parts per million nitrogenous contaminants (varying by flow rate, duration of bubbling, and the amount of solvent in the reactor) can be introduced into the experiment. This scenario of nitrogenous contamination results in levels of NH_3 that are much higher than the synthesized NH_3 concentration reported in most pNRR studies (Figure 1B). This makes feed gas pretreatment an essential decontamination step. Although most current studies acknowledge the importance of gas pretreatment, there is still a lack of consensus on the specific methods used to treat gases. This has resulted in the adoption of various approaches in different studies. The absence of systematic discussions evaluating the effectiveness of different gas treatment methods has prevented standardization. Here, we select the three most common pretreatments used in aqueous-based pNRR studies (water trap, acid trap, and alkaline trap) and evaluate their cleaning effects by comparing the levels of NH_3, NO_2^-, and NO_3^- in the reactor after bubbling.

Deionized (DI) water (water trap), 0.05 M H_2SO_4 (acid trap), or 0.1 M KOH with 0.1 M $KMnO_4$ (alkaline trap) was added to the gas-washing bottles as gas traps that were connected to a reactor with 30 mL DI water. Ultra-high-purity N_2 gas flowed continuously for 4.5 h through the gas trap and then the reactor at a rate of 50 SCCM. The flow rate, the amount of solution in the reactor, and the total duration of the bubbling are set to be identical to those used in subsequent photocatalysis experiments. The results show that the concentrations of NH_3 and NO_2^- are quite low (Figure 2A), averaging around 3 ppb even without any treatment. This makes NH_3 and NO_2^- unlikely to be the main contributors to contamination. However, the content of NO_3^- is relatively high, being two orders of magnitude greater than that of NH_3 and NO_2^-, around 0.1 ppm without any treatment. In both eNRR and pNRR, NO_3^- has been identified as a nitrogenous contaminant that cannot be overlooked, as it is thermodynamically easier to form NH_3 from NO_3^- compared to N_2.[21,34,39] Therefore, for pNRR studies with NH_3 concentrations that fall within this range, extra care is required. Our findings indicate that the alkaline trap exhibits better decontamination efficacy to remove NO_3^-. This is consistent with previous studies suggesting that the alkaline trap can stabilize gaseous NO_x intermediates, thus retaining them in the gas trap.[34] It is worth noting that these contamination levels may vary depending on experimental conditions. Therefore, we recommend using the alkaline trap for aqueous systems and reporting the concentrations of nitrogenous contaminants after purification as a reference for future pNRR research.

In addition, we custom-built a stainless-steel photoreactor (Figure 2B), with all nitrogen-free components (Figures S1 and S2; Table S2). The photoreactor is designed not only to prevent potential contamination from nitrogen-containing materials but also to minimize exposure to the environment during sampling, thus reducing the risk of contamination. Moreover, the photoreactor is equipped with a water jacket connected to a water circulation system to regulate the temperature during the reaction. Under our experimental conditions, the temperature of 30 mL of DI water can increase by ~10°C after irradiation with a 300-W Xenon lamp (full spectrum) for 4 h (Figure S3). Considering the potential impact of temperature on catalytic performance, we maintained the temperature at 23°C throughout photocatalytic testing. Furthermore, we strictly adhere to a customized cleaning

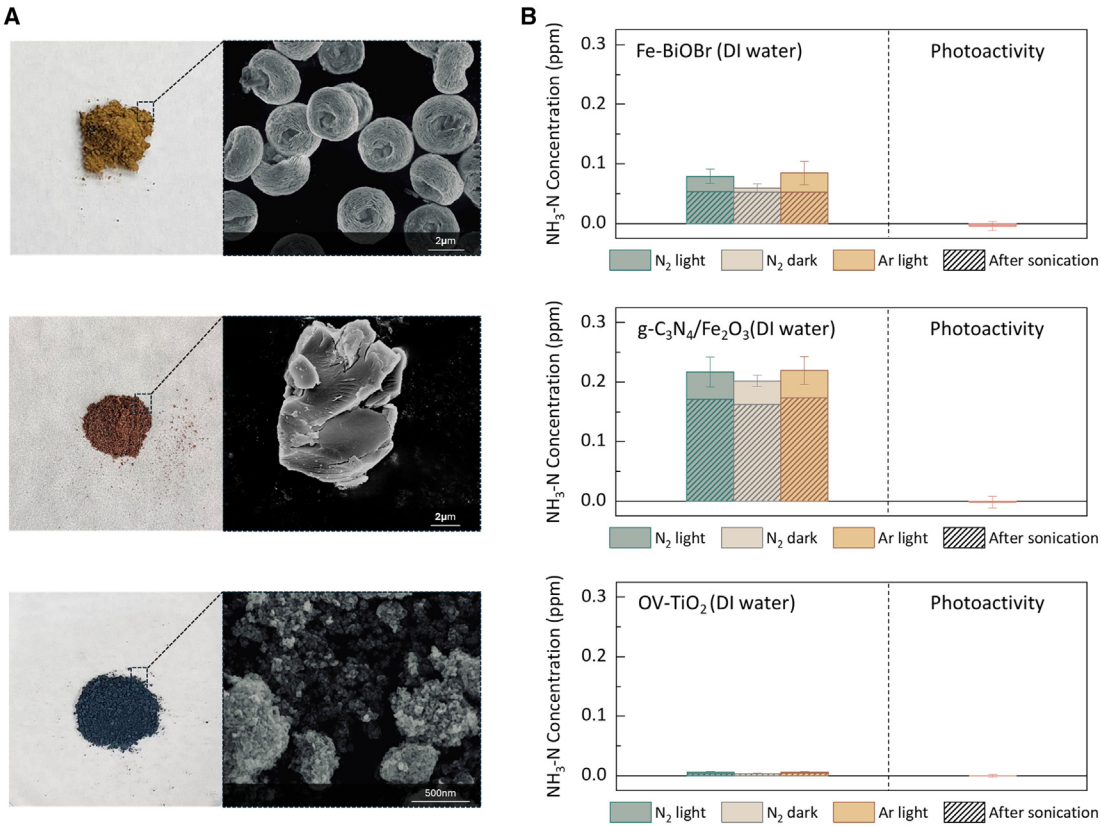

Figure 3. Photoactivities under benchmarking conditions

(A) Pictures and scanning electron microscopy (SEM) images of Fe-BiOBr, g-C_3N_4/Fe_2O_3, and OV-TiO_2 photocatalysts.

(B) Photocatalytic activity of Fe-BiOBr, g-C_3N_4/Fe_2O_3, and OV-TiO_2 in DI water under various conditions. The photoactivity of the material is obtained by subtracting the NH_3 measured in the N_2 light experiment from that measured in the Ar light experiment. N_2 light and Ar light were collected after full-spectrum irradiation for 4 h in N_2 or Ar environments. N_2 dark was collected in a dark N_2 environment for 4 h. Photocatalysts were sonicated in solution for 30 min prior to all experiments to ensure better dispersion. The diagonal hatched areas represent the ammonia levels in the solution after dispersion. The error bars represent the SDs from three independent experiments.

procedure (Figure S4) between experiments. This cleaning procedure includes sonication and rinsing with an ethanol solution (10 vol %), an alkaline solution (0.1 mM KOH), and fresh DI water, and shows better decontamination effectiveness compared to rinsing with DI water only (Figure S5). This process aims to eradicate any organic or inorganic nitrogenous contaminants that may remain from previous experimental runs. Our system consists of a gas flow meter, an alkaline trap, a water trap, and a custom-built reactor (Figure S6). Adding all these efforts toward decontamination (gas treatment and rigorous cleaning), the background concentration of NH_3 in our system during blank tests (without the presence of a photocatalyst) is ~1 ppb. The low-concentration NH_3 allows us to exclude the impact of adventitious nitrogen contamination when examining catalyst activity.

Bismuth oxyhalides (BiOX, where X = Cl, Br, I), graphitic carbon nitrides (g-C_3N_4), and defective-TiO_2 are the most commonly reported classes of materials in current pNRR research (Figure 1B; Table S1). Here, we selected three representative photocatalysts from these materials to synthesize and test: Fe-BiOBr, g-C_3N_4/Fe_2O_3, and OV-TiO_2 (Figure 3A). X-ray diffraction, X-ray photoelectron spectroscopy, and energy-dispersive X-ray spectroscopy were performed to verify the formation of the target materials (Figures S7–S9). Before transfer to the photoreactor, 30 mg of the as-prepared photocatalyst was mixed with 30 mL DI water, followed by 30 min of sonication to ensure proper dispersion of the photocatalyst in the solution. The solution was bubbled with N_2 or Ar for 30 min in the photoreactor, which was then continuously flushed with N_2 or Ar under full-spectrum irradiation, denoted as N_2 light and Ar light, respectively. A control experiment was conducted under the same conditions as N_2 light, with the only difference being the absence of the light source, denoted as N_2 dark. The results show that under the same N_2 environment, the samples exposed to light (N_2 light) show an increase in the concentration of NH_3 compared to the samples kept in the dark (N_2 dark) (Figure 3B). In addition, the observed color change in the solution provides additional evidence that photochemical reactions occur under irradiation (Figures S10–S12). However, a similar increase in NH_3 concentration was observed in both N_2 light and Ar light experiments. One possible explanation is that the photogenerated NH_3 we measured originates from the photoconversion of nitrogen-containing impurities (N impurities) rather than pNRR. Furthermore, the concentration of NH_3 in the solution

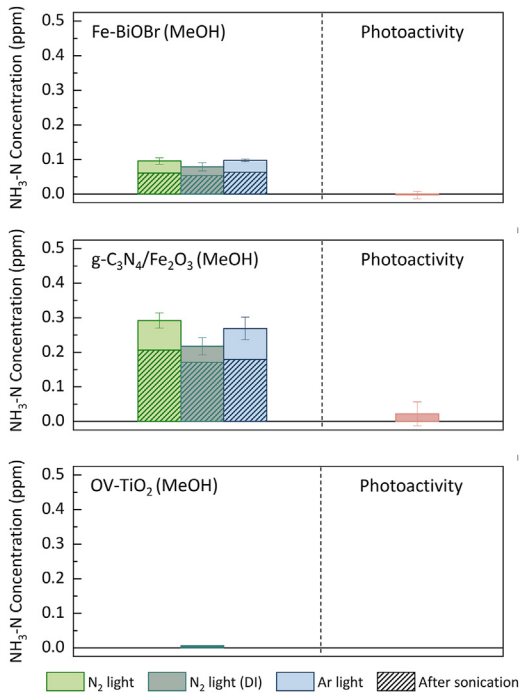

Figure 4. False positive results originate from hole scavenger

Photocatalytic activity of Fe-BiOBr, g-C_3N_4/Fe_2O_3, and OV-TiO_2 in 10 vol % methanol solution or DI water under various conditions. The photoactivity of the material is obtained by subtracting the NH_3 measured in the N_2 light experiment from that measured in the Ar light experiment. N_2 light and Ar light were collected after full-spectrum irradiation for 4 h in N_2 or Ar environments. The photocatalysts were sonicated in solution for 30 min prior to all experiments to ensure better dispersion. The diagonal hatched areas represent the ammonia levels in the solution after dispersion. The error bars represent the SDs from three independent experiments.

increased after sonication, especially in the cases of Fe-BiOBr and g-C_3N_4/Fe_2O_3. This also suggests that these photocatalysts introduced nitrogenous contamination (Figure S13). Nitrogenous contamination could be attributed to the use of urea and nitrates as precursors for these two catalysts, which convert to NH_3 and other N impurities (including but not limited to NO_2^- and NO_3^-) during the high-temperature synthesis process. The NH_3 and N impurities remaining in the photocatalyst are released into the DI water during the sonication step, leading to an increase in NH_3 concentration prior to irradiation. Upon exposure to light, the N impurities transform into NH_3, resulting in similar NH_3 concentrations in both N_2 light and Ar light. In particular, all materials were subjected to three rounds of cleaning with ethanol and DI water after synthesis, which is the widely adopted procedure for cleaning photocatalysts according to the literature.[40–43] Our results suggest that materials synthesized from nitrogen-containing precursors require extra caution during cleaning. If the NH_3 difference between the N_2 light and Ar light experiments is not significant (at least an order of magnitude difference), then the concentrations of NH_3, NO_2^-, and NO_3^- prior to irradiation should be measured and reported.

The standard benchmark tests presented in Figure 3B utilized a pure aqueous solvent (i.e., DI water). However, hole scavengers are widely used to suppress recombination and increase photoactivity.[44–46] Methanol is commonly used in pNRR studies as a hole scavenger (Table S1). Experiments carried out in 10 vol % methanol solution show a higher concentration of NH_3 than those carried out in DI water (Figure 4). Specifically, in both Fe-BiOBr and g-C_3N_4/Fe_2O_3, the NH_3 concentrations increase by 22% and 32%, respectively. However, if we conduct the same photocatalytic experiment but replace N_2 with Ar, a similar increase in NH_3 can be observed. The adventitious NH_3 content in the 10 vol % methanol solution was measured to be less than 1 ppb (Figure S14), suggesting that the increase in the concentration of NH_3 is probably due to other N impurities present in the methanol solution, which can be converted into NH_3 through photoconversion, rather than through the photoreduction of N_2 into NH_3. Similar false positive results are observed even using high-purity methanol from different suppliers (Figure S14). One hypothesis is that the increase in NH_3 originates from the photoconversion of NO_3^-, since we have detected the existence of NO_3^- in the methanol solution from the ion chromatography measurement (Figure S15). However, whether NO_3^- is the impurity that leads to false positive results requires further verification and is beyond the scope of this work. Our results here show that methanol (or organic hole scavengers in general) may contain N impurities. We recommend that for future studies involving hole scavengers, conducting an Ar control in a solution containing the same hole scavenger (referred to as the hole scavenger Ar control) is essential to validate the hole scavenger effect.

Our photocatalytic test results indicate that these three materials (Fe-BiOBr, g-C_3N_4/Fe_2O_3, and OV-TiO_2) are not active for the pNRR under these conditions. This work does not aim to refute the theoretical feasibility of pNRR, as it is thermodynamically viable,[21] but suggests that the results in the literature might not be repeatable under the carefully controlled conditions reported here. Furthermore, these results do not conflict with spectroscopic evidence that dinitrogen is activated or reduced in the presence of carbon on TiO_2,[47,48] but they do indicate that these carbon-mediated reactions with N_2 likely do not result in the catalytic formation of NH_3. We also acknowledge that the catalytic performance of materials is closely related to the synthesis process. Slight changes in material properties, such as the ratio of surface to bulk defects, may result in different pNRR performances.[49,50] Therefore, we do not intend to discredit these previous reports since we cannot confirm that our materials are identical. We seek to reiterate the importance of rigorous testing procedures, encourage independent reproducibility testing between groups, and suggest researchers submit errata if their results cannot be reproduced under carefully controlled conditions in their own labs.

As awareness of contamination issues continues to grow, an increasing number of studies in this field are reporting that isotope-labeling NMR results support the production of photofixed NH_3. However, the $^{15}N_2$ gas itself carries isotopic contamination.[26,51] The NMR spectrum (Figure 5) shows that solutions bubbled with 98% $^{15}N_2$, the most used isotopic N_2 gas in the field, exhibit clear doubled peaks (corresponding to 1.16 ppm of $^{15}NH_3$) without irradiation. Pretreating $^{15}N_2$ with an alkaline trap (0.1 M KOH with 0.1 M $KMnO_4$) can effectively prevent the interference of adventitious $^{15}NH_3$. Based on our results, strict

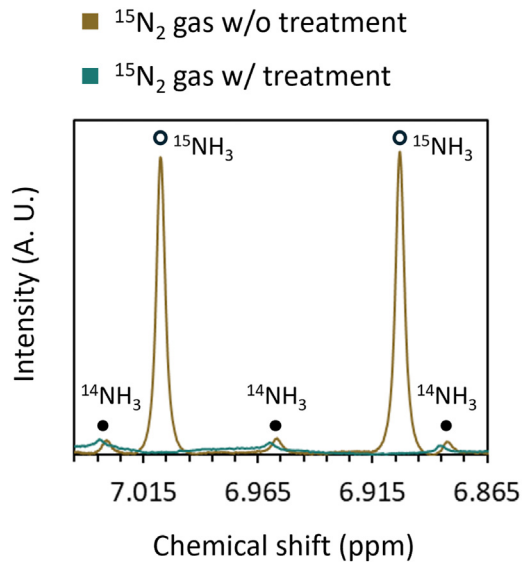

Figure 5. Presence of $^{15}NH_3$ contamination in commercial $^{15}N_2$ gas

The NH_3 contamination in commercial $^{15}N_2$ gas measured by ^1H NMR. The experimental setup was identical to that of a N_2 dark control experiment, with and without gas treatment (alkaine trap). The $^{14}NH_3$ is derived from the commercial p25 TiO_2, which was used as the photocatalyst in this set of experiments.

gas treatment for $^{15}N_2$ gas is necessary. If $^{15}N_2$ gas is not pretreated, then simply reporting the characteristic double peaks from ^1H NMR measurements is insufficient to verify the origin of NH_3 because it could be introduced from impurities in the $^{15}N_2$ gas. Currently, the most rigorous standard is still the quantitative isotopic analysis, where the NH_3 concentration measured by isotope-labeling NMR should align with the results of other measurements (e.g., ion chromatography, the colorimetric method).[52] We also recommend including isotopic NMR results obtained without irradiation (referred to as isotopic dark control) to ensure the absence of $^{15}NH_3$ contamination from $^{15}N_2$.

Conclusion

Adventitious NH_3 and N impurities obscure the study of the photoactivity of catalysts in pNRR. Here, we examine possible sources of contamination: (1) feed gas flowing into the system, (2) precursors used in the synthesis of catalysts, and (3) hole scavenger used during reaction. The three catalysts (Fe-BiOBr, g-C_3N_4/Fe_2O_3, and OV-TiO_2) evaluated with our custom-built photoreactor, cleaning protocol, and control experiments did not show photoactivity toward pNRR. We aim to raise awareness of the importance of control experiments in elucidating the photoactivity of catalysts for pNRR. We suggest (1) introducing gas treatments (e.g., alkaline trap) to the system to pretreat the feed gases (including isotopically labeled N_2), (2) rigorously cleaning the catalyst before using it and reporting nitrogenous contamination prior to irradiation, (3) performing a hole scavenger Ar control experiment to confirm the hole scavenger effect, and (4) employing quantitative isotopically labeled NMR experiments with pretreated $^{15}N_2$ gas and conducting an isotopic dark control to confirm the absence of $^{15}NH_3$. Although these steps require considerable time and resources, they are critical to ensuring the reliability and reproducibility of reported pNRR activity.

EXPERIMENTAL PROCEDURES

Photocatalytic experiments

The photocatalytic performance of the selected photocatalysts (as-prepared OV-TiO_2, Fe-BiOBr, g-C_3N_4/Fe_2O_3, or commercial p25 TiO_2) was evaluated under full-spectrum irradiation, using a 300-W Xenon lamp (Newport Corporation) as the light source. In a typical experiment, 30 mg photocatalysts was added to 30 mL solution (i.e., DI water or 10 vol % methanol solution), followed by 30 min of sonication to obtain a well-dispersed mixture. The mixture was then transferred to our custom-built photoreactor (Figures S1 and S2). The photoreactor was equipped with a water recirculation attachment to maintain a constant temperature of 23°C. The mixture was continuously stirred in the dark (200 rpm) while ultra-high-purity N_2 or Ar was bubbled through the solution at a flow rate of 50 SCCM for 30 min to obtain a saturated aqueous solution. To avoid contamination from the feed gases (N_2 and Ar), the gases were pretreated through an alkaline trap (0.1 M $KMnO_4$ in 0.1 M KOH) to remove adventitious ammonia and NO_x. The photoreactor was then continuously aerated with N_2 or Ar at a 50-SCCM flow rate under full-spectrum irradiation with continuous stirring. For dark control experiments, the experimental setup was identical to that of the N_2 light experiment, except without the exposure to light. The setup for the $^{15}N_2$ contamination experiment, shown in Figure 5, was very similar to the dark control experiment, except that the nitrogen gas ($^{14}N_2$) was switched to isotope-labeled $^{15}N_2$ gas. After 30 min of bubbling, we turned off the gas flow and closed both the gas inlet and outlet of the photoreactor to make it a closed system. The cleaning of the photoreactor strictly follows the cleaning procedure (Figure S4) we established before every experiment. Additionally, all other equipment, including vials, tubes, filters, cuvettes, and caps, were cleaned with DI water to suppress ammonia contamination before every experiment (and measurement). To measure the pNRR products, ion chromatography (Figure S16) and NMR (Figure S17) were used for NH_3 detection and UV-vis spectroscopy was used for NO_2^- (Figure S18) and NO_3^- (Figure S19) measurements.

RESOURCE AVAILABILITY

Lead contact

Requests for further information and resources should be directed to and will be fulfilled by the lead contact, Marta C. Hatzell (marta.hatzell@me.gatech.edu).

Materials availability

This study did not generate new materials.

Data and code availability

This study did not generate any datasets.

ACKNOWLEDGMENTS

This work was supported by the National Science Foundation under grant nos. 1846611, 1943707, and 1933646. This work was supported by the Gordon and Betty Moore Foundation (Award 10615). This work was also supported by the Center for Advancing Sustainable and Distributed Fertilizer Production (CASFER), National Science Foundation under grant no. EEC-2133576. D.A.C.H. was partially supported by the RBI Graduate Research Fellowship from the Renewable Bioproducts Institute at Georgia Institute of Technology. We acknowledge Prof. Faisal M. Alamgir from the School of Materials Science and Engineering at the Georgia Institute of Technology for his assistance in the analysis and the discussion of material characterizations.

AUTHOR CONTRIBUTIONS

M.C.H. and A.J.M. supervised the project. P.-W.H. and D.A.C.H. conceived the idea, designed and performed the experiments, and synthesized the materials. P.-W.H., D.A.C.H., and H.S. conducted the material characterizations. All authors contributed to the data analysis, writing, review, and editing.

DECLARATION OF INTERESTS

The authors declare no competing interests.

DECLARATION OF GENERATIVE AI AND AI-ASSISTED TECHNOLOGIES IN THE WRITING PROCESS

During the preparation of this work, the authors used ChatGPT for grammar check. After using this tool, the authors reviewed and edited the content as needed and take full responsibility for the content of the publication.

SUPPLEMENTAL INFORMATION

Supplemental information can be found online at https://doi.org/10.1016/j.checat.2024.101128.

Received: June 26, 2024
Revised: August 7, 2024
Accepted: September 5, 2024
Published: October 2, 2024

REFERENCES

1. Sachs, J.D., and Warner, A.M. (1999). The big push, natural resource booms and growth. J. Dev. Econ. *59*, 43–76. https://doi.org/10.1016/S0304-3878(99)00005-X.
2. Rouwenhorst, K.H.R., Travis, A.S., and Lefferts, L. (2022). 1921–2021: A Century of Renewable Ammonia Synthesis. Sustain. Chem. *3*, 149–171. https://doi.org/10.3390/suschem3020011.
3. Russel, D.A., and Williams, G.G. (1977). History of Chemical Fertilizer Development. Soil Sci. Soc. Am. J. *41*, 260–265. https://doi.org/10.2136/sssaj1977.03615995004100020020x.
4. Dhar, N., Seshacharyulu, E., and Biswas, N. (1941). New aspects of nitrogen fixation and loss in soils. Proc. Natl. Inst. Sci. India *7*, 115–131.
5. Schrauzer, G.N., and Guth, T.D. (1977). Photolysis of water and photoreduction of nitrogen on titanium dioxide. J. Am. Chem. Soc. *99*, 7189–7193. https://doi.org/10.1021/ja00464a015.
6. Soria, J., Conesa, J.C., Augugliaro, V., Palmisano, L., Schiavello, M., and Sclafani, A. (1991). Dinitrogen photoreduction to ammonia over titanium dioxide powders doped with ferric ions. J. Phys. Chem. *95*, 274–282. https://doi.org/10.1021/J100154A052.
7. Augugliaro, V., Lauricella, A., Rizzuti, L., Schiavello, M., and Sclafani, A. (1982). Conversion of solar energy to chemical energy by photoassisted processes—I. Preliminary results on ammonia production over doped titanium dioxide catalysts in a fluidized bed reactor. Int. J. Hydrogen Energy *7*, 845–849. https://doi.org/10.1016/0360-3199(82)90001-5.
8. Augugliaro, V., D'Alba, F., Rizzuti, L., Schiavello, M., and Sclafani, A. (1982). Conversion of solar energy to chemical energy by photoassisted processes—II. Influence of the iron content on the activity of doped titanium dioxide catalysts for ammonia photoproduction. Int. J. Hydrogen Energy *7*, 851–855. https://doi.org/10.1016/0360-3199(82)90002-7.
9. Edwards, J.G., Davies, J.A., Boucher, D.L., and Mennad, A. (1992). An Opinion on the Heterogeneous Photoreactions of N2 with H2O. Angew. Chem. Int. Ed. Engl. *31*, 480–482. https://doi.org/10.1002/anie.199204801.
10. Augugliaro, V., and Soria, J. (1993). Concerning "An Opinion on the Heterogeneous Photoreduction of N2 with H2O": First Letter. Angew. Chem. Int. Ed. Engl. *32*, 550. https://doi.org/10.1002/anie.199305501.
11. Palmisano, L., Schiavello, M., and Sclafani, A. (1993). Concerning "An Opinion on the Heterogeneous Photoreduction of N2 with H2O": Second Letter. Angew. Chem. Int. Ed. Engl. *32*, 551. https://doi.org/10.1002/anie.199305511.
12. Davies, J.A., and Edwards, J.G. (1993). Reply: Standards of Demonstration for the Heterogeneous Photoreactions of N2 with H2O. Angew. Chem. Int. Ed. Engl. *32*, 552–553. https://doi.org/10.1002/anie.199305521.
13. David, W.; others (2020). Ammonia: Zero-Carbon Fertiliser, Fuel and Energy Store (Policy Brief).
14. Van der Hoeven, M., Kobayashi, Y., and Diercks, R. (2013). Technology roadmap: Energy and GHG reductions in the chemical industry via catalytic processes. Int. Energy Agency Paris *56*. https://www.iea.org/reports/technology-roadmap-energy-and-ghg-reductions-in-the-chemical-industry-via-catalytic-processes.
15. David, W.I.F., Agnew, G.D., Bañares-Alcántara, R., Barth, J., Bøgild Hansen, J., Bréquigny, P., De Joannon, M., Fürstenberg Stott, S., Fürstenberg Stott, C., Guati-Rojo, A., et al. (2024). 2023 roadmap on ammonia as a carbon-free fuel. JPhys Energy *6*, 021501. https://doi.org/10.1088/2515-7655/ad0a3a.
16. Schiffer, Z.J., and Manthiram, K. (2017). Electrification and Decarbonization of the Chemical Industry. Joule *1*, 10–14. https://doi.org/10.1016/j.joule.2017.07.008.
17. Hatzell, M.C. (2024). The Colors of Ammonia. ACS Energy Lett. *9*, 2920–2921. https://doi.org/10.1021/acsenergylett.4c01391.
18. Schlögl, R. (2003). Catalytic synthesis of ammonia—a "never-ending story". Angew. Chem. Int. Ed. *42*, 2004–2008. https://doi.org/10.1002/anie.200301553.
19. Fernandez, C., Chapman, O., Brown, M., and Hatzell, M. (2024). Cost competitiveness of blue and green ammonia in future energy markets. Preprint at ChemRxiv. https://doi.org/10.26434/chemrxiv-2024-b38rz.
20. Comer, B.M., Fuentes, P., Dimkpa, C.O., Liu, Y.-H., Fernandez, C.A., Arora, P., Realff, M., Singh, U., Hatzell, M.C., and Medford, A.J. (2019). Prospects and Challenges for Solar Fertilizers. Joule *3*, 1578–1605. https://doi.org/10.1016/j.joule.2019.05.001.
21. Medford, A.J., and Hatzell, M.C. (2017). Photon-Driven Nitrogen Fixation: Current Progress, Thermodynamic Considerations, and Future Outlook. ACS Catal. *7*, 2624–2643. https://doi.org/10.1021/acscatal.7b00439.
22. Liu, Y.-H., Fernández, C.A., Varanasi, S.A., Bui, N.N., Song, L., and Hatzell, M.C. (2021). Prospects for aerobic photocatalytic nitrogen fixation. ACS Energy Lett. *7*, 24–29. https://doi.org/10.1021/acsenergylett.1c02260.
23. Song, H., Chipoco Haro, D.A., Huang, P.-W., Barrera, L., and Hatzell, M.C. (2023). Progress in Photochemical and Electrochemical C–N Bond Formation for Urea Synthesis. Acc. Chem. Res. *56*, 2944–2953. https://doi.org/10.1021/acs.accounts.3c00424.
24. Brown, K.A., Harris, D.F., Wilker, M.B., Rasmussen, A., Khadka, N., Hamby, H., Keable, S., Dukovic, G., Peters, J.W., Seefeldt, L.C., and King, P.W. (2016). Light-driven dinitrogen reduction catalyzed by a CdS:nitrogenase MoFe protein biohybrid. Science *352*, 448–450. https://doi.org/10.1126/science.aaf2091.
25. Zhu, D., Zhang, L., Ruther, R.E., and Hamers, R.J. (2013). Photo-illuminated diamond as a solid-state source of solvated electrons in water for nitrogen reduction. Nat. Mater. *12*, 836–841. https://doi.org/10.1038/nmat3696.
26. Andersen, S.Z., Čolić, V., Yang, S., Schwalbe, J.A., Nielander, A.C., McEnaney, J.M., Enemark-Rasmussen, K., Baker, J.G., Singh, A.R., Rohr, B.A., et al. (2019). A rigorous electrochemical ammonia synthesis protocol with quantitative isotope measurements. Nature *570*, 504–508. https://doi.org/10.1038/s41586-019-1260-x.
27. Iriawan, H., Andersen, S.Z., Zhang, X., Comer, B.M., Barrio, J., Chen, P., Medford, A.J., Stephens, I.E.L., Chorkendorff, I., and Shao-Horn, Y. (2021). Methods for nitrogen activation by reduction and oxidation. Nat. Rev. Methods Primers *1*, 56. https://doi.org/10.1038/s43586-021-00053-y.
28. Li, H., Shang, J., Ai, Z., and Zhang, L. (2015). Efficient Visible Light Nitrogen Fixation with BiOBr Nanosheets of Oxygen Vacancies on the Exposed {001} Facets. J. Am. Chem. Soc. *137*, 6393–6399. https://doi.org/10.1021/jacs.5b03105.
29. Hirakawa, H., Hashimoto, M., Shiraishi, Y., and Hirai, T. (2017). Photocatalytic conversion of nitrogen to ammonia with water on surface oxygen vacancies of titanium dioxide. J. Am. Chem. Soc. *139*, 10929–10936. https://doi.org/10.1021/jacs.7b06634.

30. Li, J., Li, H., Zhan, G., and Zhang, L. (2017). Solar Water Splitting and Nitrogen Fixation with Layered Bismuth Oxyhalides. Acc. Chem. Res. *50*, 112–121. https://doi.org/10.1021/acs.accounts.6b00523.

31. Zhang, D., He, W., Ye, J., Gao, X., Wang, D., and Song, J. (2021). Polymeric Carbon Nitride-Derived Photocatalysts for Water Splitting and Nitrogen Fixation. Small *17*, 2005149. https://doi.org/10.1002/smll.202005149.

32. Hao, Y.-C., Chen, L.-W., and Yin, A.-X. (2022). Reply to: Reassessment of the catalytic activity of bismuth for aqueous nitrogen electroreduction. Nat. Catal. *5*, 385–387. https://doi.org/10.1038/s41929-022-00786-3.

33. Choi, J., Du, H.-L., Chatti, M., Suryanto, B.H.R., Simonov, A.N., and MacFarlane, D.R. (2022). Reassessment of the catalytic activity of bismuth for aqueous nitrogen electroreduction. Nat. Catal. *5*, 382–384. https://doi.org/10.1038/s41929-022-00785-4.

34. Choi, J., Suryanto, B.H.R., Wang, D., Du, H.-L., Hodgetts, R.Y., Ferrero Vallana, F.M., MacFarlane, D.R., and Simonov, A.N. (2020). Identification and elimination of false positives in electrochemical nitrogen reduction studies. Nat. Commun. *11*, 5546. https://doi.org/10.1038/s41467-020-19130-z.

35. Zhao, Y., Shi, R., Bian, X., Zhou, C., Zhao, Y., Zhang, S., Wu, F., Waterhouse, G.I.N., Wu, L.-Z., Tung, C.-H., and Zhang, T. (2019). Ammonia Detection Methods in Photocatalytic and Electrocatalytic Experiments: How to Improve the Reliability of NH3 Production Rates? Adv. Sci. *6*, 1802109. https://doi.org/10.1002/advs.201802109.

36. Wang, W., Zhang, H., Zhang, S., Liu, Y., Wang, G., Sun, C., and Zhao, H. (2019). Potassium-ion-assisted regeneration of active cyano groups in carbon nitride nanoribbons: visible-light-driven photocatalytic nitrogen reduction. Angew. Chem. Int. Ed. *58*, 16644–16650. https://doi.org/10.1002/anie.201908640.

37. Gao, X., Wen, Y., Qu, D., An, L., Luan, S., Jiang, W., Zong, X., Liu, X., and Sun, Z. (2018). Interference Effect of Alcohol on Nessler's Reagent in Photocatalytic Nitrogen Fixation. ACS Sustain. Chem. Eng. *6*, 5342–5348. https://doi.org/10.1021/acssuschemeng.8b00110.

38. Huang, P.-W., and Hatzell, M.C. (2022). Prospects and good experimental practices for photocatalytic ammonia synthesis. Nat. Commun. *13*, 7908. https://doi.org/10.1038/s41467-022-35489-7.

39. Comer, B.M., and Medford, A.J. (2018). Analysis of Photocatalytic Nitrogen Fixation on Rutile TiO2(110). ACS Sustain. Chem. Eng. *6*, 4648–4660. https://doi.org/10.1021/acssuschemeng.7b03652.

40. Zhao, Y., Zhao, Y., Shi, R., Wang, B., Waterhouse, G.I.N., Wu, L.-Z., Tung, C.-H., and Zhang, T. (2019). Tuning Oxygen Vacancies in Ultrathin TiO2 Nanosheets to Boost Photocatalytic Nitrogen Fixation up to 700 nm. Adv. Mater. *31*, 1806482. https://doi.org/10.1002/adma.201806482.

41. Zhang, S., Zhao, Y., Shi, R., Zhou, C., Waterhouse, G.I.N., Wu, L.-Z., Tung, C.-H., and Zhang, T. (2020). Efficient Photocatalytic Nitrogen Fixation over Cuδ+-Modified Defective ZnAl-Layered Double Hydroxide Nanosheets. Adv. Energy Mater. *10*, 1901973. https://doi.org/10.1002/aenm.201901973.

42. Zhang, S., Zhao, Y., Shi, R., Zhou, C., Waterhouse, G.I.N., Wang, Z., Weng, Y., and Zhang, T. (2021). Sub-3 nm Ultrafine Cu2O for Visible Light Driven Nitrogen Fixation. Angew. Chem. Int. Ed. *60*, 2554–2560. https://doi.org/10.1002/anie.202013594.

43. Liu, Y., Hu, Z., and Yu, J.C. (2020). Fe Enhanced Visible-Light-Driven Nitrogen Fixation on BiOBr Nanosheets. Chem. Mater. *32*, 1488–1494. https://doi.org/10.1021/acs.chemmater.9b04448.

44. Zhang, G., Yang, X., He, C., Zhang, P., and Mi, H. (2020). Constructing a tunable defect structure in TiO 2 for photocatalytic nitrogen fixation. J. Mater. Chem. A *8*, 334–341. https://doi.org/10.1039/C9TA10471B.

45. Cao, S., Zhou, N., Gao, F., Chen, H., and Jiang, F. (2017). All-solid-state Z-scheme 3,4-dihydroxybenzaldehyde-functionalized Ga2O3/graphitic carbon nitride photocatalyst with aromatic rings as electron mediators for visible-light photocatalytic nitrogen fixation. Appl. Catal. B Environ. *218*, 600–610. https://doi.org/10.1016/j.apcatb.2017.07.013.

46. Yao, C., Wang, R., Wang, Z., Lei, H., Dong, X., and He, C. (2019). Highly dispersive and stable Fe 3+ active sites on 2D graphitic carbon nitride nanosheets for efficient visible-light photocatalytic nitrogen fixation. J. Mater. Chem. A *7*, 27547–27559. https://doi.org/10.1039/C9TA09201C.

47. Huang, P.-W., Tian, N., Rajh, T., Liu, Y.-H., Innocenti, G., Sievers, C., Medford, A.J., and Hatzell, M.C. (2023). Formation of carbon-induced nitrogen-centered radicals on titanium dioxide under illumination. JACS Au *3*, 3283–3289. https://doi.org/10.1021/jacsau.3c00556.

48. Comer, B.M., Liu, Y.-H., Dixit, M.B., Hatzell, K.B., Ye, Y., Crumlin, E.J., Hatzell, M.C., and Medford, A.J. (2018). The Role of Adventitious Carbon in Photo-catalytic Nitrogen Fixation by Titania. J. Am. Chem. Soc. *140*, 15157–15160. https://doi.org/10.1021/jacs.8b08464.

49. Zou, X., Liu, J., Su, J., Zuo, F., Chen, J., and Feng, P. (2013). Facile Synthesis of Thermal- and Photostable Titania with Paramagnetic Oxygen Vacancies for Visible-Light Photocatalysis. Chem. Eur J. *19*, 2866–2873. https://doi.org/10.1002/chem.201202833.

50. Han, Q., Wu, C., Jiao, H., Xu, R., Wang, Y., Xie, J., Guo, Q., and Tang, J. (2021). Rational design of high-concentration Ti3+ in porous carbon-doped TiO2 nanosheets for efficient photocatalytic ammonia synthesis. Adv. Mater. *33*, 2008180. https://doi.org/10.1002/adma.202008180.

51. Dabundo, R., Lehmann, M.F., Treibergs, L., Tobias, C.R., Altabet, M.A., Moisander, P.H., and Granger, J. (2014). The contamination of commercial 15N2 gas stocks with 15N-labeled nitrate and ammonium and consequences for nitrogen fixation measurements. PLoS One *9*, e110335. https://doi.org/10.1371/journal.pone.0110335.

52. Huang, P.-W., Song, H., Yoo, J., Chipoco Haro, D.A., Lee, H.M., Medford, A.J., and Hatzell, M.C. (2024). Impact of Local Microenvironments on the Selectivity of Electrocatalytic Nitrate Reduction in a BPM-MEA System. Adv. Energy Mater. *14*. https://doi.org/10.1002/aenm.202304202.

Chem Catalysis, Volume *4*

Supplemental information

Benchmarking photocatalysts

for dinitrogen photoreduction reaction

Po-Wei Huang, Danae A. Chipoco Haro, Hakhyeon Song, Andrew J. Medford, and Marta C. Hatzell

Supplemental experimental procedures

Materials

Anatase TiO_2 (powder 99.98%), p25 TiO_2 (nanopowder, 21 nm primary particle size (TEM), ≥99.5% trace metals basis), $NaBH_4$ (ReagentPlus®,99%), KBr (ACS reagent, 99.0%), KOH (ACS reagent, >85%), ethanol (200 proof, 99.5%), $FeCl_3$ (98%), urea (ACS reagent, 99.0-100.5%), melamine (99%), $^{14}NH_4Cl$ (ACS reagent, ≥99.5%), $^{15}NH_4Cl$ (≥98 atom % ^{15}N, ≥99% (CP)), $^{15}N_2$ gas (98 atom%), methanesulfonic acid (≥99%), $Fe(NO_3)_3 \cdot 9\ H_2O$ (ACS reagent, ≥98%), poly(ethylene glycol) (average Mn 400), $KMnO_4$ (ACS reagent, ≥99.0%), phosphoric acid (85 wt.% in H2O), N-(1-Naphthyl) ethylenediamine dihydrochloride (>98%), p-aminobenzenesulfonamide (≥98%), nitrite standard solution (40.0 mg L^{-1} NO_2-N in H2O), nitrate standard solution (40.0 mg L^{-1} NO_3-N in H_2O), H_2SO_4 (ACS reagent, 95.0-98.0%), and sulfamic acid (ACS reagent, 99.3%) were obtained from Sigma-Aldrich. Ultra-high-purity N_2 and ultra-high-purity Ar were purchased from Airgas. Dimethyl sulfoxide (DMSO-d6, 99.9%) was purchased from Cambridge Isotope Laboratories. Methanol were obtained from Burdick & Jackson™ (>99.9%) and from VWR Chemicals (>99.8%) and from Sigma-Aldrich (>99.9%). Hydrochloric acid (HCl, assay 30%) was purchased from Spectrum Chemical Mfg. Corp. All purchased materials were used as received without any additional purification steps.

Preparation of photocatalysts

Synthesis of OV-TiO_2. The mixture of commercial anatase TiO_2 and $NaBH_4$ in equal mass loading was heated in a ceramic boat at 340°C (heating rate 5°C min^{-1}) in a tubular furnace (MTI Corporation, OTF-1200X) under Ar atmosphere for 30 minutes. Before the reaction, the as-synthesized catalyst was cleaned with DI water and ethanol three times respectively. The procedure was adopted from literature.

Synthesis of Fe-BiOBr. Add 1.5 mmol KBr and 0.45 mmol of $Fe(NO_3)_3\ 9\ H_2O$ to 18 mL of poly(ethylene glycol) and stir for 4h. Transfer to an Autoclave Reactor (Huanyu WJJ-263A, 20 mL) and place it in muffle furnace (Quincy Lab, Inc., Model 30 Lab Oven) at 120°C. Before the reaction, the as-synthesized catalyst was cleaned with DI water and ethanol three times respectively. The procedure was adopted from literature.

Synthesis of g-C_3N_4/Fe_2O_3. Stirr 1.6g of $FeCl_3$, 7.2g of urea, and 0.96g of melamine in an oil bath at 95°C. Heat the liquid at 550°C (heating ramp: 3°C min^{-1}) in a tubular furnace (MTI Corporation, OTF-1200X) for 4 hours. The as-synthesized catalyst was wash with DI water and ethanol three times respectively, and dry in a muffle furnace (Quincy Lab, Inc., Model 30 Lab Oven) at 60°C. The procedure was adopted from literature.

Materials characterizations

X-ray spectroscopy (XPS) measurements were performed using Thermo K-Alpha (Thermo Fisher Scientific) with an Al K-α (1.486 KeV) source, 400 μm spot size, and 50 eV of pass energy. The flood gun was used in all the measurements. The binding energy was calibrated with C1s spectrum on the C-C peak at 284.8 eV.

X-ray diffraction (XRD) measurements were performed using MiniFlex600 (Rigaku) with an Cu K-α source (λ =1.54056 ˚A).

Scanning electron microscopy (SEM) elucidated the morphology of the material using Hitachi SU-8230 SEM with an accelerating voltage of 5 kV and energy-dispersive spectroscopy (EDS) mapping (Oxford EDS detector) was conducted with an accelerating voltage of 15 kV.

Gas pretreated experiments

The setup for the gas pretreated experiments was identical to the N_2 dark experiment, except for the absence of photocatalysts. Deionized water (DI water), 0.05 M H_2SO_4 (acid trap), or 0.1 M KOH with 0.1 M $KMnO_4$ (alkaline trap)[1] were added to gas washing bottles as gas traps, which were connected to the photoreactor containing 30 mL of DI water. Ultra-high-purity N_2 flowed continuously for 4.5 hours through the gas trap and then the reactor at a rate of 50 SCCM. The solution in the photoreactor was collected after bubbling and measured using ion chromatography (for ammonia) and UV-vis spectroscopy (for nitrite and nitrate).

Measurements of pNRR products

Ammonia (IC)

5 mL of the reaction mixture was collected after photocatalysis experiment and passed through a PTFE syringe filter (Foxx Life Sciences) to obtain a transparent solution for the ammonia measurement. The concentration of ammonia in the solution was determined by Dionex Aquion ion chromatography (Thermofisher) coupled with CS12A cation exchange column (for DI water solution), 20 mM methanesulfonic acid was used as the eluent passing through the column with a flow rate of 0.25 mL/min. For solutions containing methanol, a CS17 cation exchange column (for 10 vol% methanol solution) was used, and 6 mM methanesulfonic acid was used as the eluent, which passed through the column at a flow rate of 0.15 mL/min. Calibration curves (Fig. S16) were made using homemade ammonia standard solutions, which were prepared by mixing ammonium chloride with DI water or a 10 vol% methanol solution.

Ammonia (NMR)

The ^{1}H NMR measurements are conducted by Bruker Advance IIIHD 700. Ammonium chloride $^{14}NH_4Cl$ (or $^{15}NH_4Cl$) was mixed with DI water to create the calibration curve for NMR measurements (Fig. S17). 1 ml of post-experiment solution was mixed with 20 uL of 0.02 M H_2SO_4. Addition of 100 µl dimethyl sulfoxide was added as the locking solution. The concentration of NH_3 is determined by the ratio of NH_3 peak area (labeled in Fig. S17) to DMSO-d6 peak area in 1H NMR.

Nitrite (UV-Vis spectroscopy)

The concentration of nitrite was obtained from UV-Vis spectroscopy using a typical colorimetric test.[2] The color reagent was prepared by dissolving 0.1 g of N-(1-Naphthyl) ethylenediamine dihydrochloride and 2 g of p-aminobenzenesulfonamide in 5 ml of phosphoric acid and 25 ml of DI water. 0.5 ml of 1 M HCl and 0.05 ml of the color reagent were added to 2.5 ml of the post-experiment solution, and the mixture was shaken to obtain a uniform solution. After 30 minutes for color development, the absorption spectrum was measured using a UV-Vis spectrophotometer at a wavelength of 540 nm. The NO_2-N calibration curves (Fig. S18) were established by mixing a nitrite standard solution with DI water.

Nitrate (UV-Vis spectroscopy)

The concentration of nitrate was obtained from UV-Vis spectroscopy following a procedure modified from ref [3]. 5 ml of the post-experiment solution was mixed with 0.1 ml of 1 M HCl and 0.01 ml of 0.8 wt% sulfamic acid solution. After 60minutes, the absorption intensities at wavelengths of 220 nm and 275 nm were recorded using quartz glass cuvettes (CV10Q14, Thorlabs) to hold the samples. The final absorbance value was calculated by this equation: $A=A_{220nm}-2*A_{275nm}$. The NO_3-N calibration curves (Fig. S19) were established by mixing a nitrate standard solution with DI water.

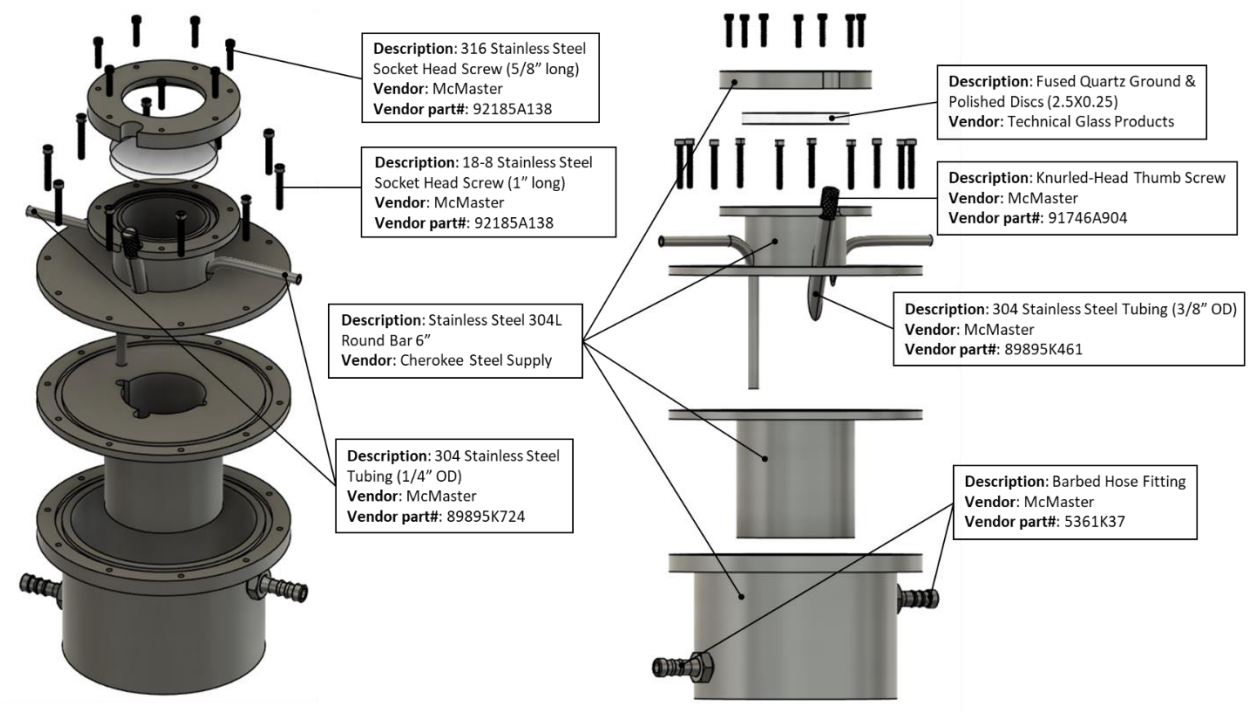

Figure S1. Schematic of the custom-built photoreactor and the recommended components for the photoreactor construction.

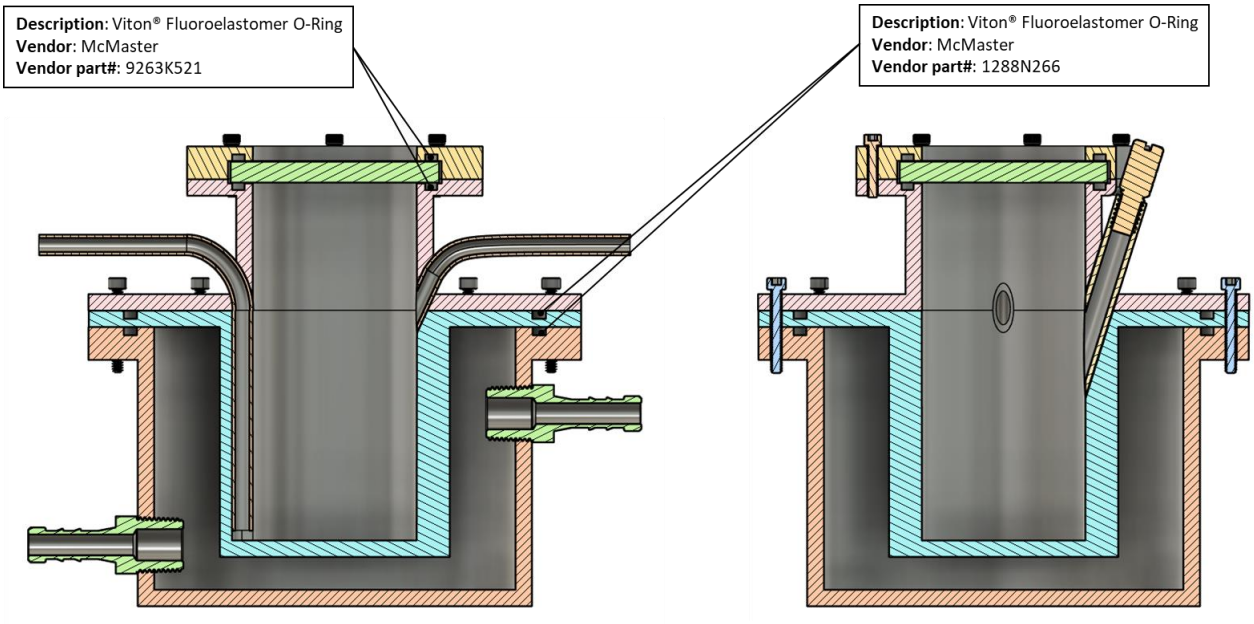

Figure S2. Cross-sectional diagram of the custom-built photoreactor and the recommended components for the photoreactor construction.

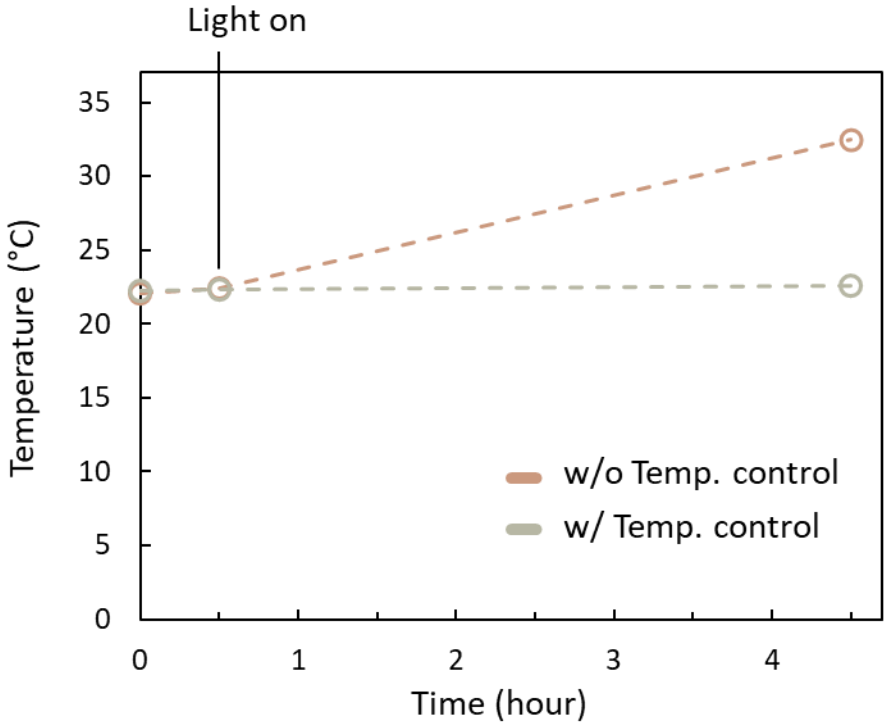

Figure S3. Temperature profiles with and without a temperature control system throughout the photocatalytic experiment.

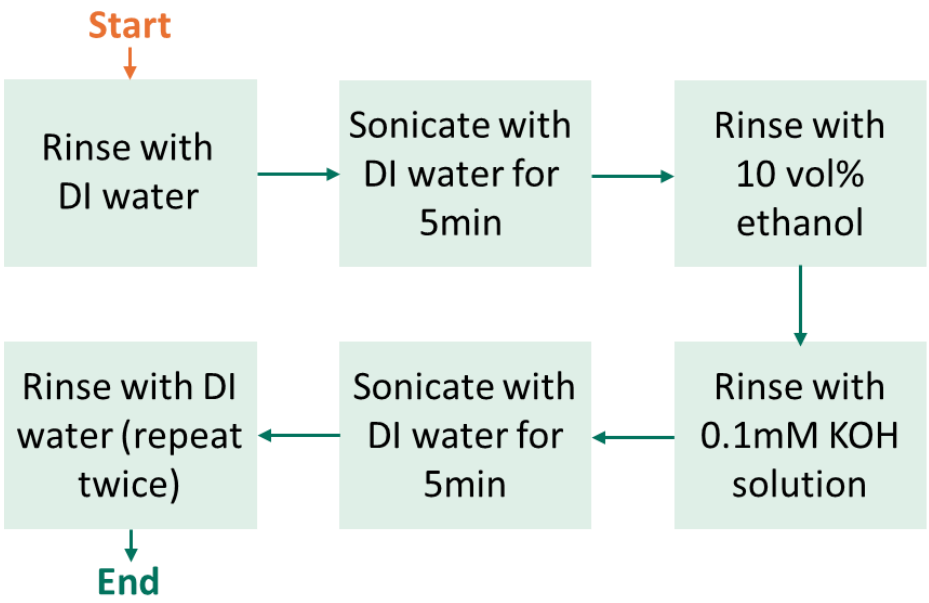

Figure S4. Recommended cleaning procedures for the photoreactor between each experiment.

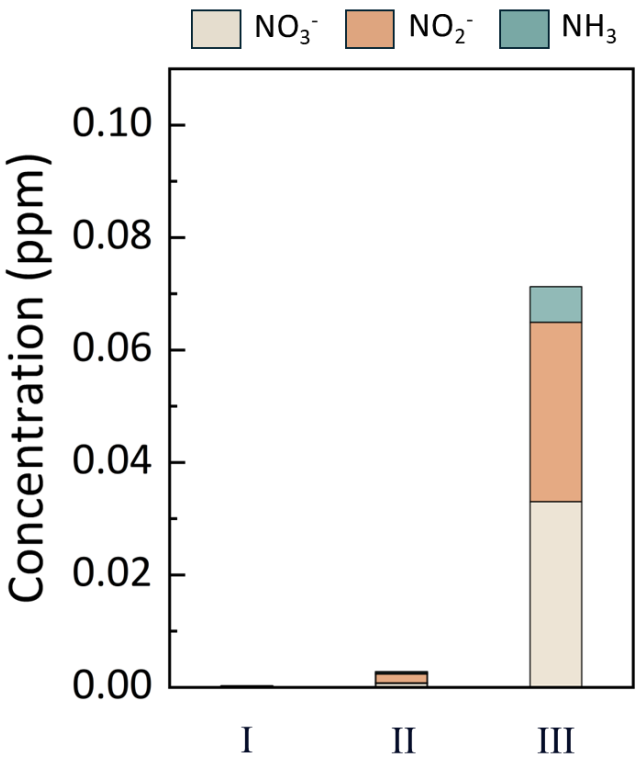

Figure S5. Decontamination effectiveness testing. 30 ml of solution containing 1 ppm NH_3-N, 1 ppm NO_2-N, and 1 ppm NO_3-N was added to the photoreactor to serve as the solution from a prior photocatalytic reaction. After removing the solution from the photoreactor, it was cleaned using (I) the recommended cleaning procedure, (II) rinsing three times with DI water, or (III) no rinsing nor cleaning procedure. Then, 30 ml of DI water was added back to the photoreactor, and the residual nitrogenous compounds were measured.

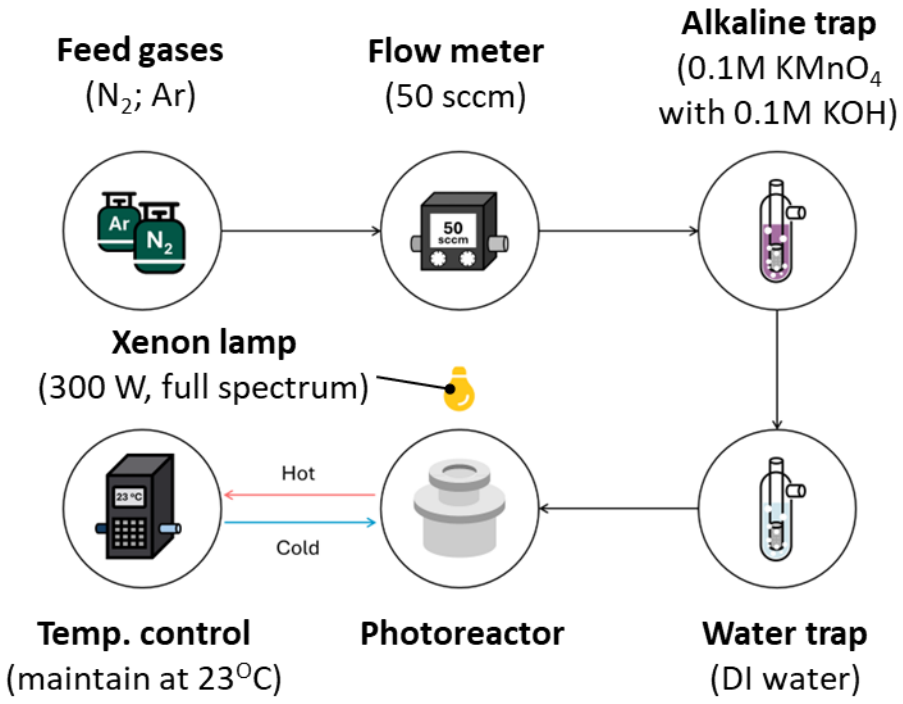

Figure S6. Flow schematic of our system setup for the pNRR experiment. The water trap installed after the alkaline trap aims to prevent the runoff of alkaline substances into the photoreactor during prolonged experiments.

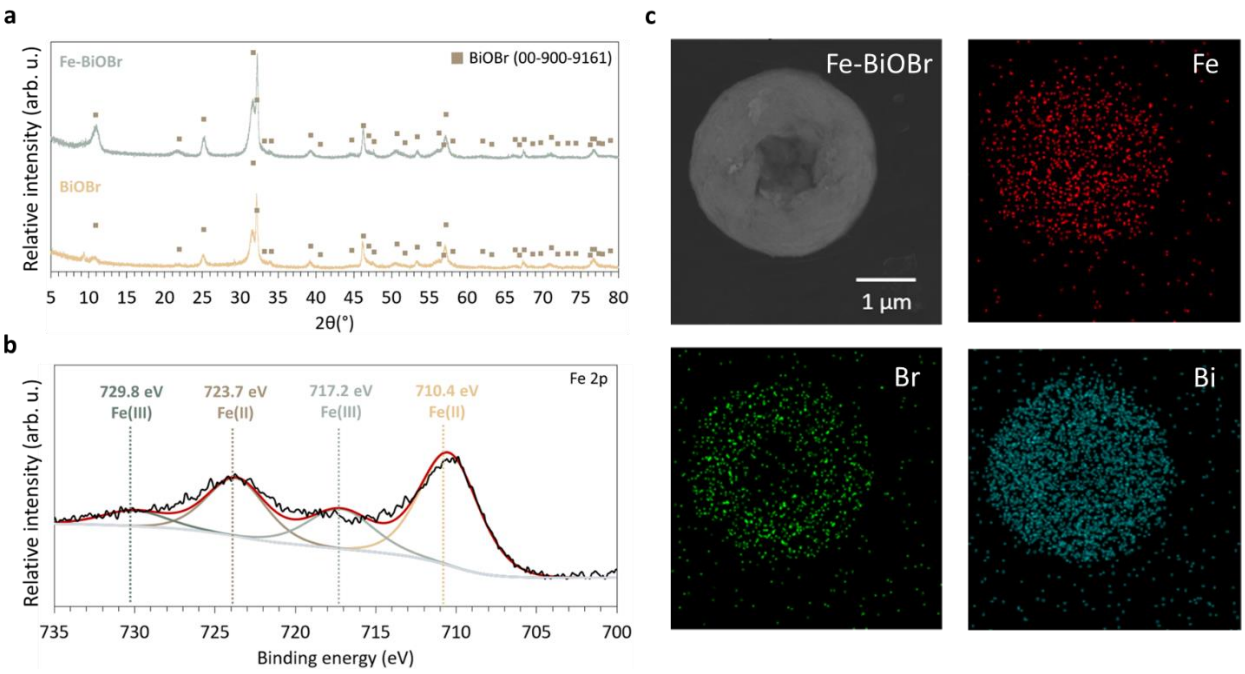

Figure S7. Material characterization for Fe-BiOBr (a) XRD patterns of Fe-BiOBr and BiOBr. (b) XPS spectra of Fe 2p, confirmed the presence of Fe in BiOBr. Fe(II) and Fe(III) are seen, Fe(II) is being formed by accepting electron from other atoms.[4] (c) EDS elemental mapping of Fe-BiOBr that shows the presence of Fe, Bi, and Br.

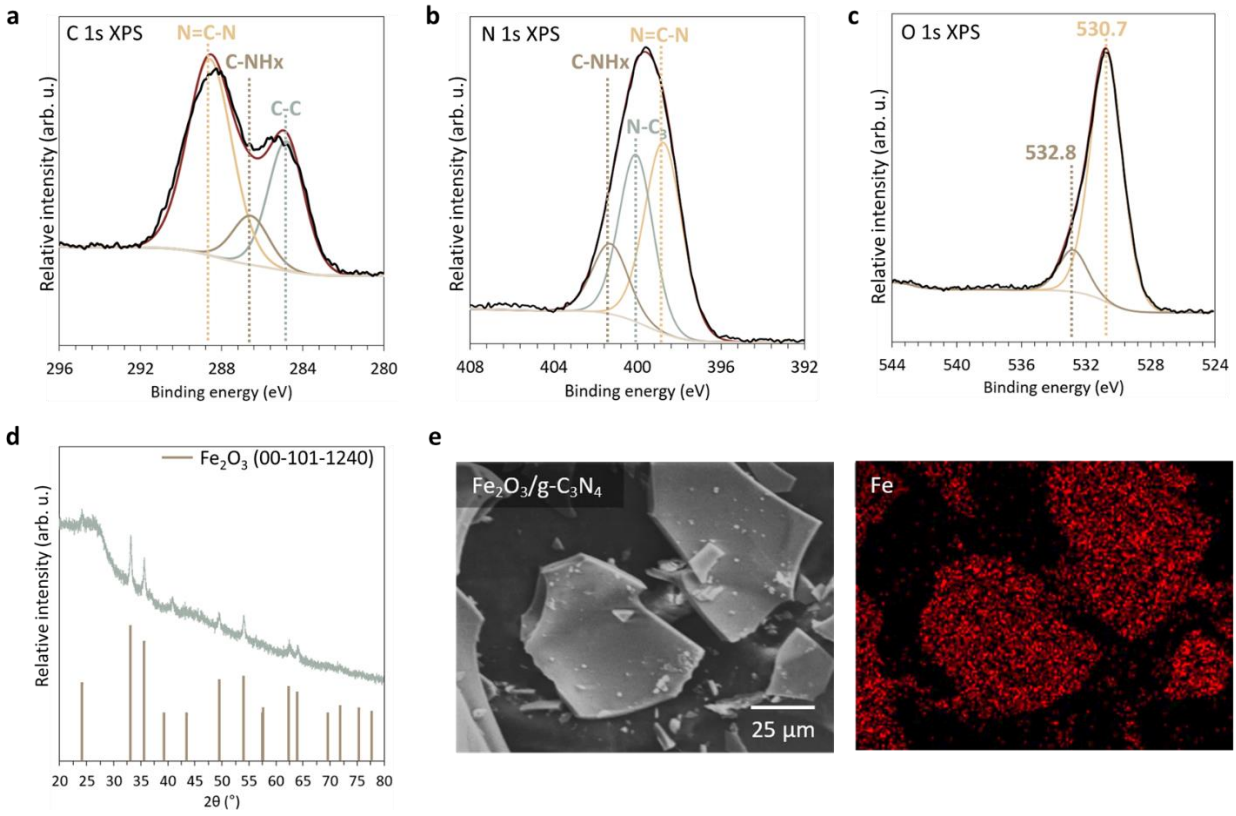

Figure S8. Material characterization for Fe_2O_3/g-C_3N_4 (a) C 1s XPS spectra of synthesized Fe_2O_3/g-C_3N_4 showing N=C-N, C-NHx, and C-C contributions to the spectra. (b) N 1s XPS spectra of synthesized Fe_2O_3/g-C_3N_4 showing N=C-N, C-NHx, and N-C_3 contributions to the spectra. (c) O 1s XPS spectra showing surface OH groups at 530.7 eV and adsorbed water at 532.8. (d) XRD pattern of Fe_2O_3/g-C_3N_4, hematite Fe_2O_3 PDF #00-101-1240 is shown as reference. (e) EDS elemental mapping of Fe_2O_3/g-C_3N_4 showing the uniform distribution of Fe.

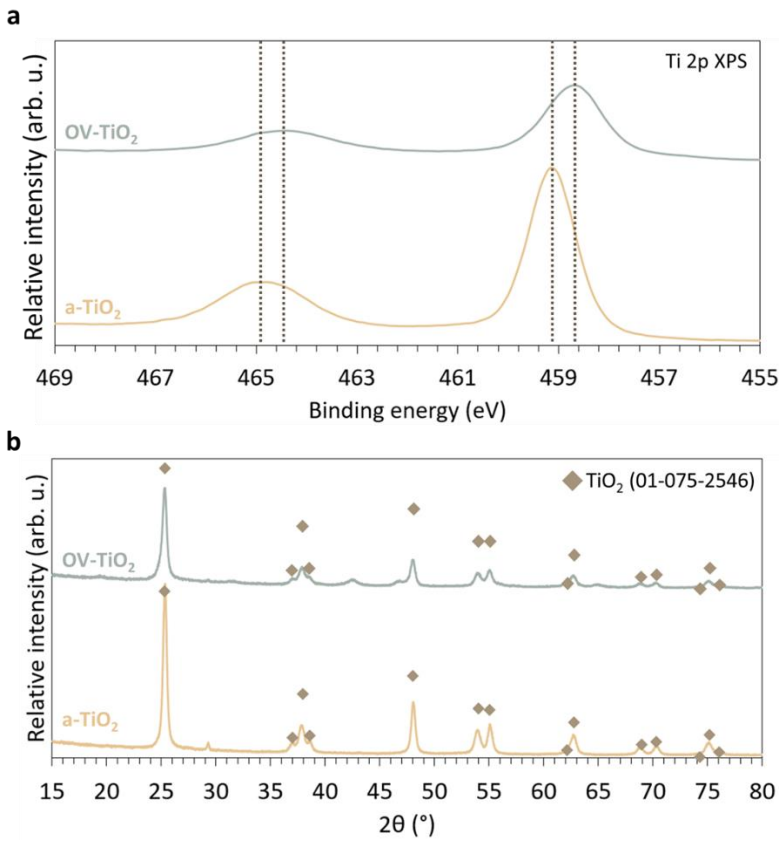

Figure S9. Material characterization for OV-TiO_2 (a) Ti 2p XPS spectra of antase-TiO_2 and OV-TiO_2. The Ti $2p_{3/2}$ and Ti $2p_{1/2}$ XPS show a 0.5eV (marked with brown dashed lines) shift to lower binding energies when OV are introduced in the Ti structure. This shift indicates the formation of Ti^{x+} species (different from Ti^{4+} from TiO_2) when OV are introduced. (b) XRD pattern of antase-TiO_2 and OV-TiO_2. TiO_2 PDF #01-075-2546 is shown as reference (diamond). When the OVs are introduced, the XRD show wider and weaker peaks because of the strains introduced in the lattice and the decrease in crystallinity.[5]

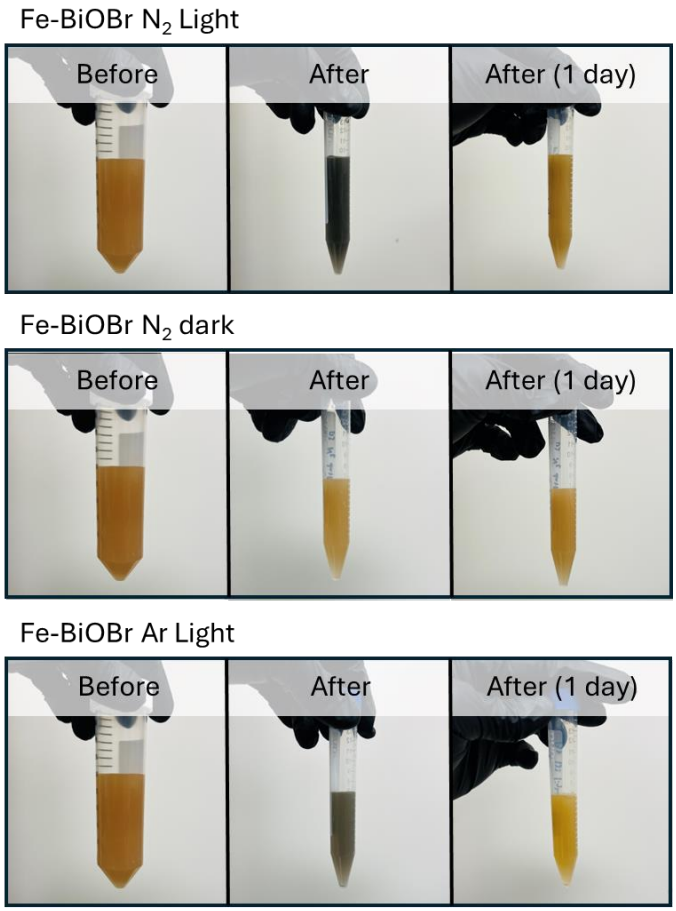

Figure S10. Pictures of Fe-BiOBr in DI water before, right after, and a day after photolysis under different experimental conditions.

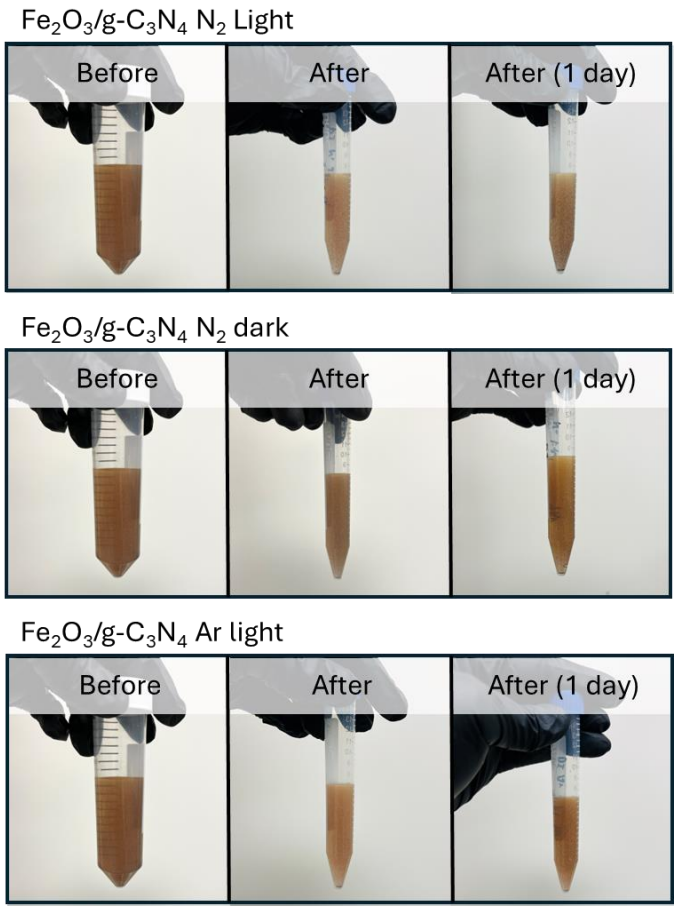

Figure S11. Pictures of Fe_2O_3/g-C_3N_4 in DI water before, right after, and a day after photolysis under different experimental conditions.

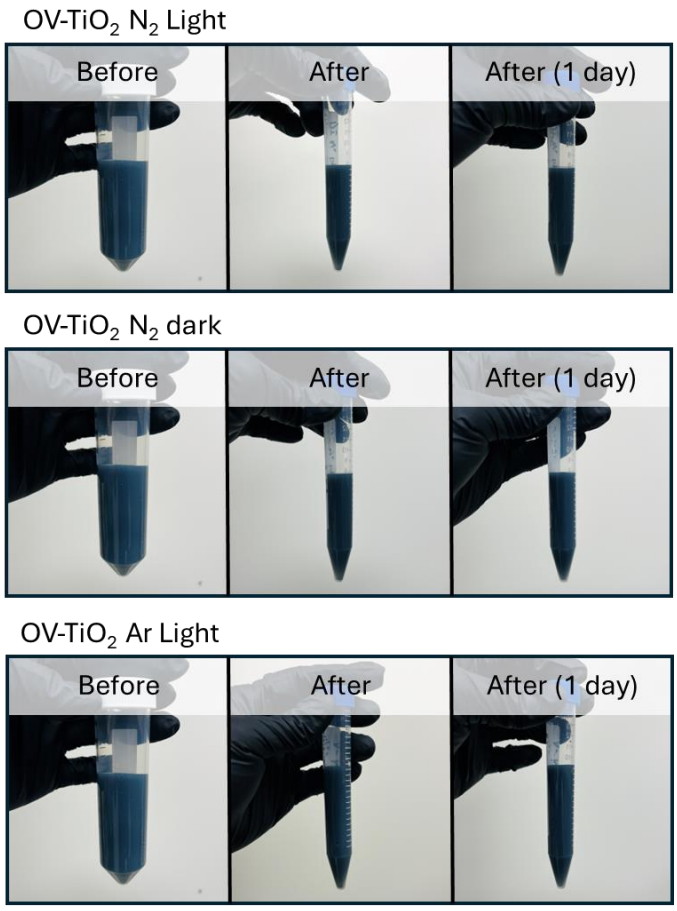

Figure S12. Pictures of OV-TiO_2 in DI water before, right after, and a day after photolysis under different experimental conditions.

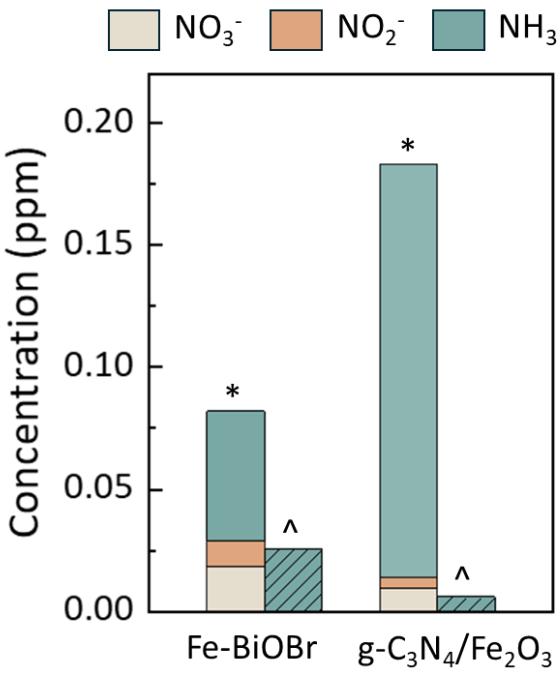

Figure S13. Nitrogenous impurities from the photocatalysts. *N impurities measured prior photocatalytic reaction. ^The ammonia difference between Ar control and dark control during photocatalytic reaction.

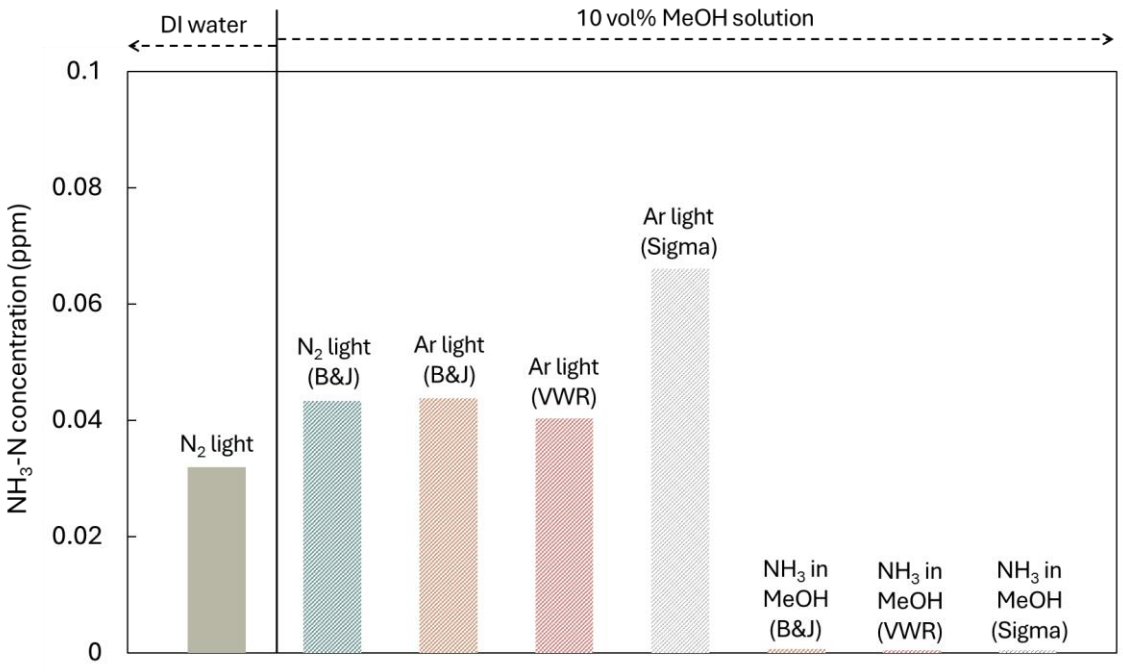

Figure S14. False-positive results from methanol solution. Methanol (>99.9% from Burdick & Jackson™ or >99.8% from VWR Chemicals or >99.9 from Sigma-Aldrich) was added to DI water to prepare a 10 vol% methanol solution for photocatalytic experiments. Commercial p25 TiO_2 was used as the photocatalyst for this set of experiments, and samples were collected after 32 hours of illumination under full spectrum. The ammonia level in the 10 vol% methanol solution was measured without the presence of photocatalysts nor illumination (denoted as NH_3 in MeOH).

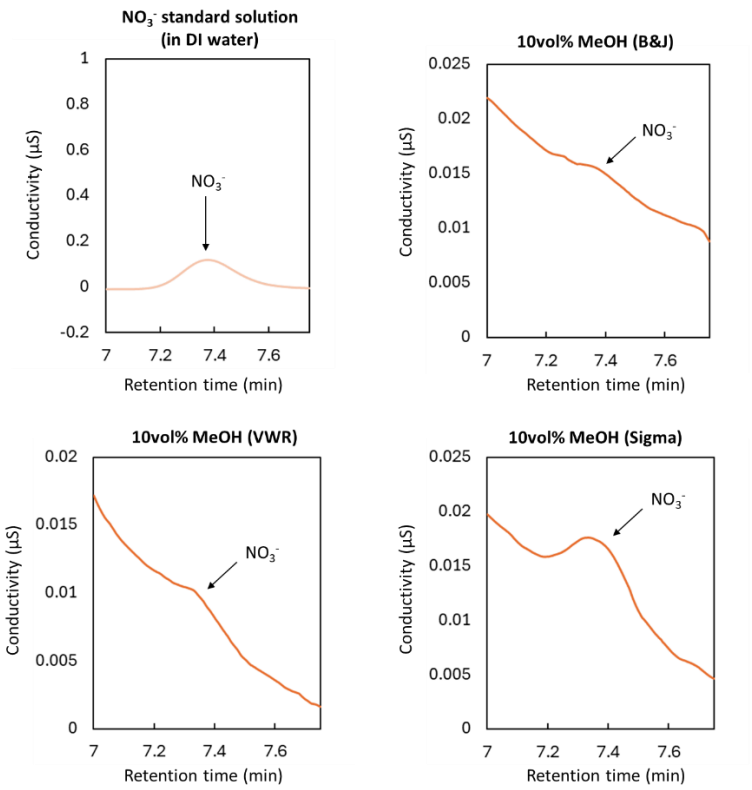

Figure S15. NO_3^- standard solution and NO_3^- measurement in 10vol% methanol solution from different vendors. The measurement is done by anionic ion chromatography.

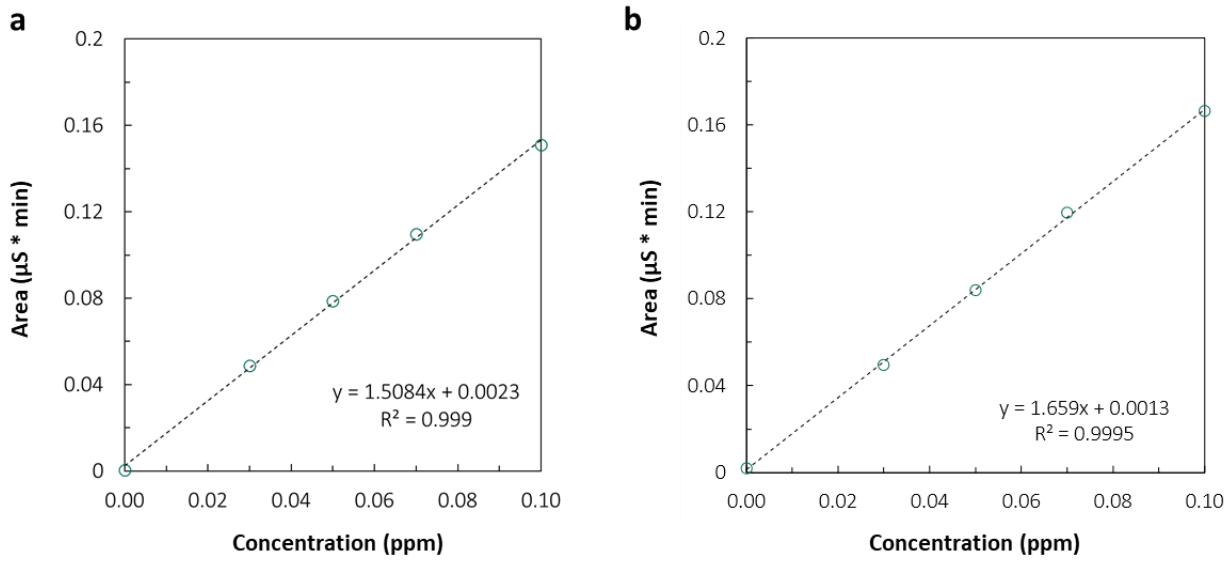

Figure S16. Calibration curves for ammonia measurement using IC in (a) DI water (b) 10 vol% methanol solution.

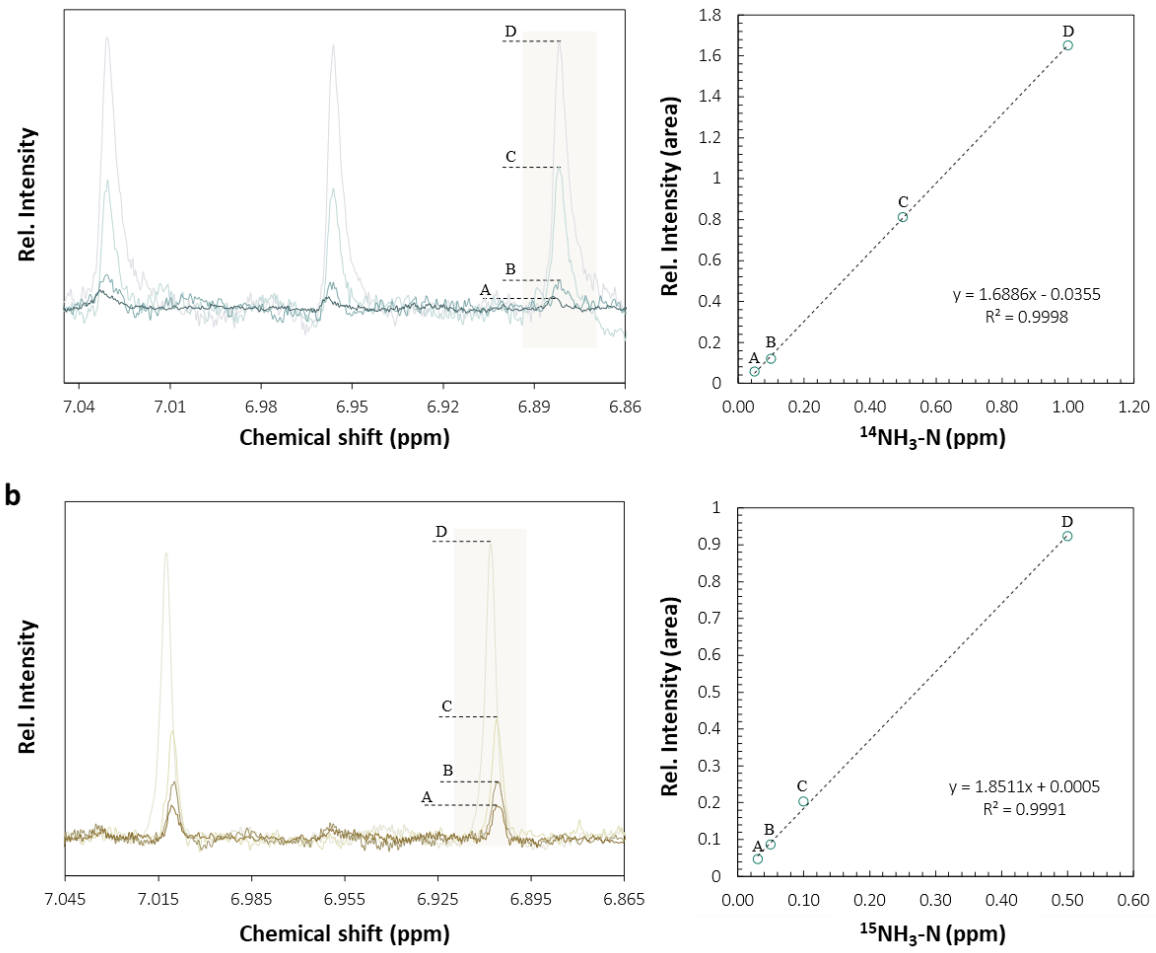

Figure S17. Calibration curves for (a) $^{14}NH_3$-N and (b) $^{15}NH_3$-N measurement using ^{1}H NMR.

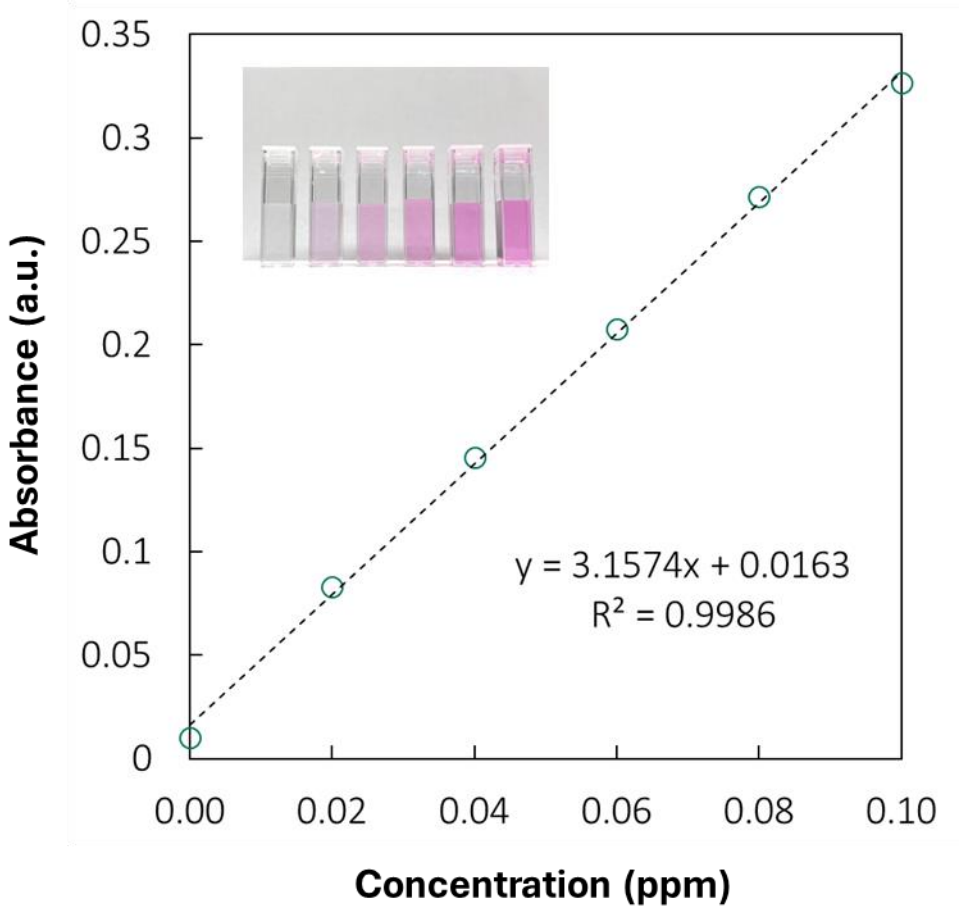

Figure S18. Calibration curves for nitrite measurement using UV-vis spectroscopy.

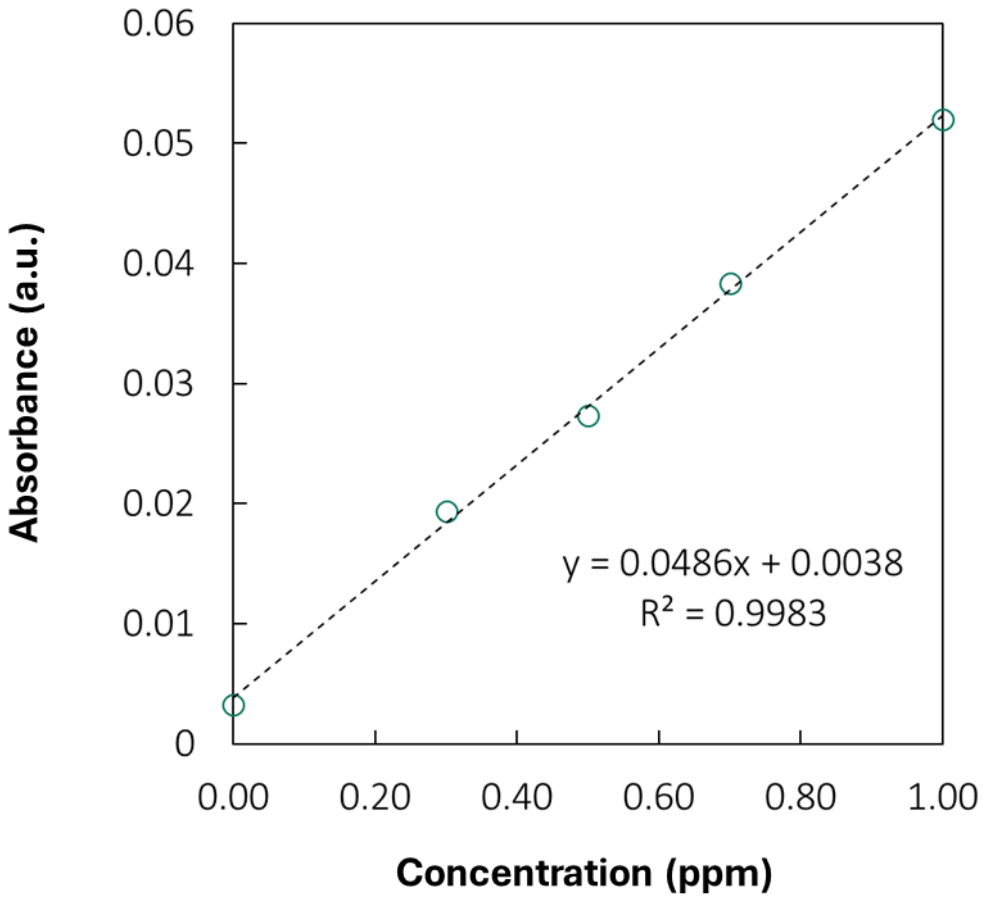

Figure S19. Calibration curves for nitrate measurement using UV-vis spectroscopy.

Supplementary Table 1. Summary of photocatalytic NRR

Catalyst	Reaction system	Light source	Hole scavenger	Flow rate (SCCM)	Gas treatment	Temp. control	Yield rate ($\mu mol\ g^{-1}\ h^{-1}$)	ppm* (mg/L)	Ref
BiOBr-OV	Solid-liquid reactor	Full specturm (300W Xe lamp)	None	60	None	O	223.3	2.01	6
D-Bi_3O_4Br	Solid-liquid reactor	Full specturm (300W Xe lamp)	None	60	None	O	50.8	0.46	7
Bi_5O_7Br-OV	Solid-liquid reactor	Visible light (300W Xe lamp)	None	50	None	X	1272	5.72	8
BiOCl-OV	Solid-liquid reactor	Full specturm (Xe lamp)	None	300	None	X	2.41	0.09	9
Fe-BiOBr	Solid-liquid reactor	Visible light (300W Xe lamp)	None	60	None	O	382.68	3.44	10
TiO_2-OV	Solid-liquid reactor	UV light (Hg lamp)	None	300	None	X	3.5	0.06	11
Au/TiO_2-OV	Solid-liquid reactor	Full specturm (300W Xe lamp)	10 vol% Methanol	50	None	X	187.1	4.21	12
Cu-TiO_2-OV	Solid-liquid reactor	Full specturm (300W Xe lamp)	None	30	None	O	78.9	1.42	13
TiO_2-OV	Solid-liquid reactor	Full specturm (300W Xe lamp)	10 vol% Methanol	N/A	None	O	324.86	2.92	14
$SrTiO_3$	Solid-liquid reactor	Full specturm (300W Xe lamp)	10 vol% Ethanol	30	Water trap	X	109.15	0.2	15
D-TiO_2	Solid-liquid reactor	Full specturm (300W Xe lamp)	None	3	None	O	178		16
WS_2@TiO_2	Solid-liquid reactor	Full specturm (300W Xe lamp)	10mM Na_2SO_3	N/A	None	X	1390		17
OV-$BaTiO_3$	Solid-liquid reactor	Full specturm (300W Xe lamp)	None	120	None	O	1043	1.88	18
OV-C/TiO_2	Solid-liquid reactor	Full specturm (300W Xe lamp)	10mM Methanol	50	None	O	84	1.51	19
C-TiO_x	Solid-liquid reactor	Visible light (300W Xe lamp)	10 vol% Methanol	30	None	O	109.3	1.97	20
Ga_2O_3-DBD/g-C_3N_4	Solid-liquid reactor	Visible light (500W Xe lamp)	0.04mM Methanol	100	None	X	281	2.02	21
BP/CN	Solid-liquid reactor	Visible light (500W Xe lamp)	5 vol% Methanol	100	None	X	579.16	6.25	22
SiW_{12}/K-C_3N_4	Solid-liquid reactor	Full specturm (Xe lamp)	None	N/A	None	X	353.2	1.59	23
S-CN-CV	Solid-liquid reactor	Full specturm (500W Xe lamp)	4 vol% Methanol	N/A	None	X	299.5	2.16	24
KOH-treated g-C_3N_4	Solid-liquid reactor	Full specturm (300W Xe lamp)	100 vol% Methanol	N/A	None	O	3632	8.72	25
Fe-EDTA–CN	Solid-liquid reactor	Visible light (300W Xe lamp)	20 vol% Methanol	100	None	X	125	0.9	26
Fe_2O_3/CN	Solid-liquid reactor	Full specturm (300W Xe lamp)	10 vol% Methanol	N/A	None	O	4380	78.84	27
Mo-CN	Solid-liquid reactor	Full specturm (300W Xe lamp)	8.33 vol% Ethanol	N/A	None	O	830	7.47	28
Au/CN-NV	Solid-liquid reactor	Visible light (300W Xe lamp)	20 vol% Methanol	50	None	X	783.4	7.05	29
B-CN	Solid-liquid reactor	Visible light (300W Xe lamp)	1mM Na_2SO_3	N/A	None	O	435.28	3.92	30
B/MoO_2-CN	Solid-liquid reactor	Visible light (300W Xe lamp)	10 vol% Methanol	N/A	None	X	1680	6.05	31
Ru-CoS-SV/CN	Solid-liquid reactor	Full specturm (300W Xe lamp)	10 vol% Methanol	N/A	None	X	438	3.94	32
BiOQD-CN	Solid-liquid reactor	Visible light (300W Xe lamp)	1mM Na_2SO_3	N/A	None	X	576.11	5.18	33

Supplementary Table 1. Summary of photocatalytic NRR

Catalyst	Reaction system	Light source	Hole scavenger	Flow rate (SCCM)	Gas treatment	Temp. control	Yield rate ($\mu mol\ g^{-1}\ h^{-1}$)	ppm* (mg/L)	Ref
Mo-$W_{18}O_{49}$	Solid-liquid reactor	Full specturm (300W Xe lamp)	1mM Na_2SO_3	30	None	X	195.5	3.519	34
In_2O_3/In_2S_3	Solid-liquid reactor	Full specturm (300W Xe lamp)	None	80	None	O	40.04	0.14	35
Cu-ZnAl-LDH	Solid-liquid reactor	Full specturm (300W Xe lamp)	None	300	None	O	110	0.1	36
BP/CdS	Solid-liquid reactor	Visible light (300W Xe lamp)	1 vol% Methanol	N/A	None	X	240.17	1.04	37
Gd-IHEP-8	Solid-liquid reactor	Full specturm (300W Xe lamp)	None	20	None	X	220	1.58	38
NH_2-MIL-125 (Ti)	Solid-liquid reactor	Full specturm (300W Xe lamp)	None	200	None	O	40	0.18	39
ZnCr-LDH	Solid-liquid reactor	Full specturm (300W Xe lamp)	None	300	None	O	33.19	0.12	40
Sb-OV	Solid-liquid reactor	Visible light (300W Xe lamp)	20 vol% Methanol	N/A	Alkaline trap (1M $NaClO_2$ + 10M NaOH)	X	20.5	0.07	41
Fe-$MoTe_2$	Solid-liquid reactor	Visible light (300W Xe lamp)	None	50	None	O	129.08	0.29	42
Au/Mo-$W_{18}O_{49}$	Solid-liquid reactor	Full specturm (300W Xe lamp)	20 vol% Methanol	30	None	X	399.24	1.48	43
Al-PMOF(Fe)	Solid-liquid reactor	Visible light (Xe lamp)	20 vol% Methanol	20	Acid trap (dilute sulfuric acid)	X	7.47	0.04	44
Cu_2O-LDH	Solid-liquid reactor	Visible light (300W Xe lamp)	None	300	None	O	30.31	0.09	45
WC-Co/NGC	Solid-liquid reactor	Full specturm (300W Xe lamp)	1mM Na_2SO_3	N/A	None	X	157	1.41	46
GDY@Fe_3O_4	Solid-liquid reactor	Visible light (300W Xe lamp)	None	N/A	Cu trap	X	1762.35	0.44	47
$Bi_2Sn_2O_7$-QD	Solid-liquid reactor	Full specturm (300W Xe lamp)	None	N/A	None	O	334.8	3.01	48
BMOF(Sr)-Fe	Solid-liquid reactor	Full specturm (300W Xe lamp)	16 wt% K_2SO_3	N/A	Cu trap (CuSAPO-34)	O	780	1.4	49
Ni_2P-BP	Solid-liquid reactor	Visible light (300W Xe lamp)	1 vol% Methanol	N/A	None	X	6.14	0.01	50
Mn-WO_3	Solid-liquid reactor	Full specturm (Xe lamp)	None	30	Acid trap (0.05M sulfuric acid)	X	425	3.83	51
S/Cu	Solid-liquid reactor	Full specturm (Xe lamp)	None	30	Cu trap (Cu-SSZ-13)	O	157	1.41	52
Au@MOF/PTFE	Gas-solid-liquid reactor	Visible light (300W Xe lamp)	None	80	None	O	360	0.57	53
CoO-Co_3O_4/RGO	Solid-liquid reactor	Full specturm (300W Xe lamp)	None	20	None	X	89.1	1.6	54
BVO/SV-ZIS	Solid-liquid reactor	Visible light (300W Xe lamp)	None	N/A	None	O	80.6	0.36	55
Ru-SA/H_xMoO_{3-y}	Solid-gas reactor	Visible light (300W Xe lamp)	None	10	None	O	4000		56

Graphitic carbon nitride; Ti-based catalysts; Bismuth oxyhalides

*The predicted ammonia level is based on the reported yield rate, volume of solution, and weight of catalyst given in the papers. The reaction time is set to one hour.

Supplementary Table 2. Components used in our system setup for the pNRR experiment

Components	Description	Vendor	Vendor part#	Note
Tubing	Bev-A-Line Transfer Tubing, Bev-A-Line® IV, 1/8" ID×1/4" OD	VWR	#MFLX06490-12	
Bubbler	Midget Impinger, Bubbler with Ace-Threds on Inlet/Outlet	Thomas Scientific	7533-18	Gas traps
Adapter	Yor-Lok Fitting for Stainless Steel Tubing	McMaster-CARR	5182K112	Connect the photoreactor with plastic tubing
On/Off Valve	High-Pressure Compact 316 Stainless Steel On/Off Valve	McMaster-CARR	45395K213	Install at the gas inlet and outlet of the photoreactor
Connector	Push-to-Connect Fitting for Plastic Tubing	McMaster-CARR	5526K92	Connect the plastic tubing
Temparature controler	MM Series Chiller	PolyScience	MM71GX1A110C	Connect the water jacket to control the temperature throughout pNRR
DI water	Ultrapure Water Purification System	Millipore Sigma	ZRQSVP3US	The DI water we used for photolysis. N contaminants (NH_3, NO_2^-, NO_3^-) were undetected at the ppb level.

Supplementary Table 3. Contamination level in different gas pretreatment methods

	NH_3 (ppm)	NO_2^- (ppm)	NO_3^- (ppm)
Water trap	Undetected	Undetected	Undetected
Acid trap*	Undetected	Undetected	Undetected
Alkaline trap^	Undetected	Undetected	Undetected

* The acid trap was diluted 50 times to meet the sample preparation requirements for our IC. ^ The alkaline trap was diluted 1000 times to meet the sample preparation requirements for our IC. The limits of detection for NH_3, NO_2^- and NO_3^- are 0.2, 0.3, and 0.6 ppb, respectively.

Supplemental References

1. Choi, J., Lee, Y., Lee, H., Kim, J., and Choi, J. (2020). Identification and elimination of false positives in electrochemical nitrogen reduction studies. Nat. Commun., 11, 5546. https://doi.org/10.1038/s41467-020-19130-z.
2. He, W., Wang, J., Zhang, Y., Liu, S., and Chen, M. (2022). Splicing the active phases of copper/cobalt-based catalysts achieves high-rate tandem electroreduction of nitrate to ammonia. Nat. Commun., 13, 1129. https://doi.org/10.1038/s41467-022-28728-4.
3. Wang, Y., Zhang, H., Wu, Y., Huang, X., and Zhao, M. (2020). Unveiling the activity origin of a copper-based electrocatalyst for selective nitrate reduction to ammonia. Angew. Chem. Int. Ed., 59, 5350–5354. https://doi.org/10.1002/anie.201915992.
4. Li, W., Zhang, S., Yu, S., and Wang, X. (2017). FeII/FeIII doped Bi/BiOBr hierarchical microspheres as a highly efficient catalyst for degradation of organic contaminants at neutral pH: the role of visible light and H2O2. ChemCatChem, 9, 3762–3771. https://doi.org/10.1002/cctc.201700549.
5. Tan, H., Yang, J., Sun, S., and Liu, L. (2014). A facile and versatile method for preparation of colored TiO2 with enhanced solar-driven photocatalytic activity. Nanoscale, 6, 10216–10223. https://10.1039/C4NR02677B
6. Li, H., Liu, J., Zhang, X., and Xu, L. (2015). Efficient visible light nitrogen fixation with BiOBr nanosheets of oxygen vacancies on the exposed {001} facets. J. Am. Chem. Soc., 137, 6393–6399. https://doi.org/10.1021/jacs.5b03105.
7. Di, J., Zhang, S., Liu, Z., and Yang, X. (2019). Defect-tailoring mediated electron–hole separation in single-unit-cell Bi3O4Br nanosheets for boosting photocatalytic hydrogen evolution and nitrogen fixation. Adv. Mater., 31, 1807576. https://doi.org/10.1002/adma.201807576.
8. Li, P., Zhang, X., Wu, Y., and Zhao, Y. (2020). Visible-light-driven nitrogen fixation catalyzed by Bi5O7Br nanostructures: enhanced performance by oxygen vacancies. J. Am. Chem. Soc., 142, 12430–12439. https://doi.org/10.1021/jacs.0c05097.
9. Shiraishi, Y., Kato, H., and Katoh, R. (2020). Photocatalytic dinitrogen fixation with water on bismuth oxychloride in chloride solutions for solar-to-chemical energy conversion. J. Am. Chem. Soc., 142, 7574–7583. https://doi.org/10.1021/jacs.0c01683.
10. Liu, Y., Hu, Z., and Yu, J.C. (2020). Fe Enhanced Visible-Light-Driven Nitrogen Fixation on BiOBr Nanosheets. Chem. Mater. 32, 1488–1494. https://doi.org/10.1021/acs.chemmater.9b04448.
11. Hirakawa, H., Kudo, A., and Saito, T. (2017). Photocatalytic conversion of nitrogen to ammonia with water on surface oxygen vacancies of titanium dioxide. J. Am. Chem. Soc., 139, 10929–10936. https://doi.org/10.1021/jacs.7b06634.
12. Yang, J., Wang, L., Zhang, X., and Yu, J. (2018). High-efficiency “working-in-tandem” nitrogen photofixation achieved by assembling plasmonic gold nanocrystals on

ultrathin titania nanosheets. J. Am. Chem. Soc., 140, 8497–8508. https://doi.org/10.1021/jacs.8b03537
13. Zhao, Y., Wang, H., and Chen, Z. (2019). Tuning oxygen vacancies in ultrathin TiO2 nanosheets to boost photocatalytic nitrogen fixation up to 700 nm. Adv. Mater., 31, 1806482. https://doi.org/10.1002/adma.201806482.
14. Zhang, G., Yang, X., He, C., Zhang, P., and Mi, H. (2020). Constructing a tunable defect structure in TiO 2 for photocatalytic nitrogen fixation. J. Mater. Chem. A 8, 334–341. https://doi.org/10.1039/C9TA10471B.
15. Huang, B., Zhang, Y., and Chen, L. (2020). Boosting the photocatalytic activity of mesoporous SrTiO3 for nitrogen fixation through multiple defects and strain engineering. J. Mater. Chem. A, 8, 22251–22256. https://doi.org/10.1039/D0TA08678A.
16. Zhang, Y., Li, Y., and Liu, S. (2020). Defective titanium dioxide nanobamboo arrays architecture for photocatalytic nitrogen fixation up to 780 nm. Chem. Eng. J., 401, 126033. https://doi.org/10.1016/j.cej.2020.126033.
17. Shi, L., Wang, W., and Zheng, X. (2020). Promoting nitrogen photofixation over a periodic WS2@ TiO2 nanoporous film. J. Mater. Chem. A, 8, 1059–1065. https://doi.org/10.1039/C9TA12743G.
18. Zhao, Z., Zhang, Y., and Xu, L. (2021). Magnetic-field-stimulated efficient photocatalytic N2 fixation over defective BaTiO3 perovskites. Angew. Chem. Int. Ed., 60, 11910–11918. https://doi.org/10.1002/anie.202100726.
19. Qian, J., Zhao, X., and Zhang, L. (2021). Photocatalytic nitrogen reduction by Ti3C2 MXene derived oxygen vacancy-rich C/TiO2. Adv. Sustainable Syst., 5, 2000282. https://doi.org/10.1002/adsu.202000282.
20. Han, Q., Zhang, Y., and Yang, Y. (2021). Rational design of high-concentration Ti3+ in porous carbon-doped TiO2 nanosheets for efficient photocatalytic ammonia synthesis. Adv. Mater., 33, 2008180. https://doi.org/10.1002/adma.202008180.
21. Cao, S., Zhang, Y., and Zhang, H. (2017). All-solid-state Z-scheme 3,4-dihydroxybenzaldehyde-functionalized Ga2O3/graphitic carbon nitride photocatalyst with aromatic rings as electron mediators for visible-light photocatalytic nitrogen fixation. Appl. Catal. B Environ., 218, 600–610. https://doi.org/10.1016/j.apcatb.2017.07.013.
22. Qiu, P., Li, J., and Wang, X. (2018). Metal-free black phosphorus nanosheets-decorated graphitic carbon nitride nanosheets with CP bonds for excellent photocatalytic nitrogen fixation. Appl. Catal. B Environ., 221, 27–35. https://doi.org/10.1016/j.apcatb.2017.09.010.
23. Xiao, C., Yang, L., and Wang, J. (2018). A new approach to enhance photocatalytic nitrogen fixation performance via phosphate-bridge: a case study of SiW12/K-C3N4. Appl. Catal. B Environ., 239, 260–267. https://doi.org/10.1016/j.apcatb.2018.08.012.

24. Cao, S., Zhang, Y., and Li, X. (2018). Sulfur-doped g-C3N4 nanosheets with carbon vacancies: General synthesis and improved activity for simulated solar-light photocatalytic nitrogen fixation. Chem. Eng. J., 353, 147–156. https://doi.org/10.1016/j.cej.2018.07.116.
25. Li, X., Zhang, X., and Zhao, L. (2018). Efficient photocatalytic fixation of N2 by KOH-treated gC3N4. J. Mater. Chem. A, 6, 3005–3011. https://doi.org/10.1039/C7TA09762J.
26. Yao, C., Liu, S., and Zhang, Y. (2019). Highly dispersive and stable Fe3+ active sites on 2D graphitic carbon nitride nanosheets for efficient visible-light photocatalytic nitrogen fixation. J. Mater. Chem. A, 7, 27547–27559. https://doi.org/10.1021/acsami.4c03370.
27. Mou, H., Wang, J., Zhang, D., Yu, D., Chen, W., Wang, D., and Mu, T. (2019). A one-step deep eutectic solvent assisted synthesis of carbon nitride/metal oxide composites for photocatalytic nitrogen fixation. J. Mater. Chem. A, 7, 5719-5725. https://doi.org/10.1039/C8TA11681D
28. Guo, X.-W., Wang, Y., and Li, Y. (2019). Single-atom molybdenum immobilized on photoactive carbon nitride as efficient photocatalysts for ambient nitrogen fixation in pure water. J. Mater. Chem. A, 7, 19831–19837. https://doi.org/10.1039/C9TA06653E.
29. Guo, Y., Zhang, X., and Yang, H. (2020). Au nanoparticle-embedded, nitrogen-deficient hollow mesoporous carbon nitride spheres for nitrogen photofixation. J. Mater. Chem. A, 8, 16218–16231. https://doi.org/10.1039/D0TA03793A.
30. Liang, C., Zhang, Y., and Li, X. (2020). Insight into photocatalytic nitrogen fixation on graphitic carbon nitride: Defect-dopant strategy of nitrogen defect and boron dopant. Chem. Eng. J., 396, 125395. https://doi.org/10.1016/j.cej.2020.125395.
31. Ran, Y., Zhang, Y., and Zhang, W. (2020). Polymeric carbon nitride with frustrated Lewis pair sites for enhanced photofixation of nitrogen. J. Mater. Chem. A, 8, 13292–13298. https://doi.org/10.1039/D0TA03914D.
32. Yuan, J., Yang, J., and Zhang, X. (2020). Efficient Photocatalytic Nitrogen Fixation: Enhanced Polarization, Activation, and Cleavage by Asymmetrical Electron Donation to N≡N Bond. Adv. Funct. Mater., 30, 1906983. https://doi.org/10.1002/adfm.201906983.
33. Liang, C., Xu, H., and Zhang, S. (2021). Efficient photocatalytic nitrogen fixation to ammonia over bismuth monoxide quantum dots-modified defective ultrathin graphitic carbon nitride. Chem. Eng. J., 406, 126868. https://doi.org/10.1016/j.cej.2020.126868.
34. Zhang, N., Wang, J., and Zhang, L. (2018). Refining defect states in W18O49 by Mo doping: a strategy for tuning N2 activation towards solar-driven nitrogen fixation. J. Am. Chem. Soc., 140, 9434–9443. https://doi.org/10.1021/jacs.8b02076.
35. Xu, H., Zhang, X., and Wang, X. (2019). Fabrication of In2O3/In2S3 microsphere heterostructures for efficient and stable photocatalytic nitrogen fixation. Appl. Catal. B Environ., 257, 117932. https://doi.org/10.1016/j.apcatb.2019.117932.

36. Zhang, S., Wang, X., and Zhang, J. (2020). Efficient photocatalytic nitrogen fixation over Cuδ+-modified defective ZnAl-layered double hydroxide nanosheets. Adv. Energy Mater., 10, 1901973. https://doi.org/10.1002/aenm.201901973.
37. Shen, Z.-K., Zheng, X., and Yang, W. (2020). Few-layer black phosphorus nanosheets: a metal-free cocatalyst for photocatalytic nitrogen fixation. ACS Appl. Mater. Interfaces, 12, 17343–17352. https://doi.org/10.1021/acsami.9b21167.
38. Hu, K.-Q., Zhang, Y., and Yang, J. (2020). Solar-Driven Nitrogen Fixation Catalyzed by Stable Radical-Containing MOFs: Improved Efficiency Induced by a Structural Transformation. Angew. Chem. Int. Ed., 59, 20666–20671. https://doi.org/10.1002/anie.202009630.
39. Huang, H., Chen, J., and Li, Y. (2020). Toward visible-light-assisted photocatalytic nitrogen fixation: A titanium metal organic framework with functionalized ligands. Appl. Catal. B Environ., 267, 118686. https://doi.org/10.1016/j.apcatb.2020.118686.
40. Zhao, Y., Zhang, S., and Li, J. (2020). Alkali etching of layered double hydroxide nanosheets for enhanced photocatalytic N2 reduction to NH3. Adv. Energy Mater., 10, 2002199. https://doi.org/10.1002/aenm.202002199.
41. Zhao, Z., Wu, Y., and Zhang, Y. (2020). Surface-engineered oxidized two-dimensional Sb for efficient visible light-driven N2 fixation. Nano Energy, 78, 105368. https://doi.org/10.1016/j.nanoen.2020.105368.
42. Li, H., Zhang, X., and Yang, J. (2020). The in-built bionic “MoFe cofactor” in Fe-doped two-dimensional MoTe2 nanosheets for boosting the photocatalytic nitrogen reduction performance. J. Mater. Chem. A, 8, 13038–13048. https://doi.org/10.1039/D0TA04251J.
43. Qiu, P., Wang, X., and Chen, L. (2021). Plasmonic gold nanocrystals simulated efficient photocatalytic nitrogen fixation over Mo doped W18O49 nanowires. J. Mater. Chem. A, 9, 14459–14465. https://doi.org/10.1039/D1TA03339E
44. Shang, S., Li, J., and Zhang, Y. (2021). Atomically dispersed iron metal site in a porphyrin-based metal–organic framework for photocatalytic nitrogen fixation. ACS Nano, 15, 9670–9678. https://doi.org/10.1021/acsnano.0c10947.
45. Zhang, S., Liu, X., and Wang, Y. (2021). Sub-3 nm ultrafine Cu2O for visible light driven nitrogen fixation. Angew. Chem. Int. Ed., 60, 2554–2560. https://doi.org/10.1002/anie.202013594.
46. Wang, L., Zhang, Y., and Wang, J. (2021). WC and cobalt nanoparticles embedded in nitrogen-doped carbon 3D nanocage derived from H3PW12O40@ ZIF-67 for photocatalytic nitrogen fixation. J. Mater. Chem. A, 9, 2912–2918. https://doi.org/10.1039/D0TA10303A.
47. Fang, Y., Chen, L., and Liu, X. (2021). Graphdiyne@ Janus magnetite for photocatalytic nitrogen fixation. Angew. Chem., 133, 3207–3211. https://doi.org/10.1002/ange.202012357.

48. Zhang, Y., Wang, H., and Zhang, X. (2021). Oxygen vacancies in Bi2Sn2O7 quantum dots to trigger efficient photocatalytic nitrogen reduction. Appl. Catal. B Environ., 299, 120680. https://doi.org/10.1016/j.apcatb.2021.120680.
49. Zhao, Z., Zhang, X., and Li, J. (2021). Boosting nitrogen activation via bimetallic organic frameworks for photocatalytic ammonia synthesis. ACS Catal., 11, 9986–9995. https://doi.org/10.1021/acscatal.1c02465.
50. Shen, Z.-K., Wang, X., and Liu, J. (2021). Identifying the role of interface chemical bonds in activating charge transfer for enhanced photocatalytic nitrogen fixation of Ni2P-black phosphorus photocatalysts. Appl. Catal. B Environ., 295, 120274. https://doi.org/10.1016/j.apcatb.2021.120274.
51. Zhang, Y., Liu, S., and Yang, X. (2021). Dual-metal sites boosting polarization of nitrogen molecules for efficient nitrogen photofixation. Adv. Sci., 8, 2100302. https://doi.org/10.1002/advs.202100302.
52. Xin, Y., Zhang, X., and Wang, J. (2021). Atomic-level insights into the activation of nitrogen via hydrogen-bond interaction toward nitrogen photofixation. Chem, 7, 2118–2136. https://doi.org/10.1016/j.chempr.2021.03.018.
53. Chen, L.-W., Zhang, Y., and Wu, Y. (2021). Metal–organic framework membranes encapsulating gold nanoparticles for direct plasmonic photocatalytic nitrogen fixation. J. Am. Chem. Soc., 143, 5727–5736. https://doi.org/10.1021/jacs.0c13342.
54. Lu, H., Wang, X., and Zhao, Y. (2022). All room-temperature synthesis, N2 photofixation and reactivation over 2D cobalt oxides. Appl. Catal. B Environ., 304, 121001. https://doi.org/10.1016/j.apcatb.2021.121001.
55. Zhang, G., Yang, X., and Li, Y. (2022). S vacancies act as a bridge to promote electron injection from Z-scheme heterojunction to nitrogen molecule for photocatalytic ammonia synthesis. Chem. Eng. J., 433, 133670. https://doi.org/10.1016/j.cej.2021.133670.
56. Yin, H., Zhang, X., and Liu, Y. (2022). Dual active centers bridged by oxygen vacancies of ruthenium single-atom hybrids supported on molybdenum oxide for photocatalytic ammonia synthesis. Angew. Chem. Int. Ed., 61, e202114242. https://doi.org/10.1002/anie.202114242.